

Geochemistry and Origin of Sulphide Minerals in Mantle Xenoliths: Qilin, Southeastern China

JINGFENG GUO^{1*}, WILLIAM L. GRIFFIN^{1,2} AND SUZANNE Y. O'REILLY^{1†}

¹ARC NATIONAL KEY CENTRE FOR GEOCHEMICAL EVOLUTION AND METALLOGENY OF CONTINENTS (GEMOC), DEPARTMENT OF EARTH AND PLANETARY SCIENCES, MACQUARIE UNIVERSITY, SYDNEY, N.S.W. 2109, AUSTRALIA

²CSIRO EXPLORATION AND MINING, P.O. BOX 136, NORTH RYDE, N.S.W. 2113, AUSTRALIA

RECEIVED FEBRUARY 11, 1998; REVISED TYPESCRIPT ACCEPTED JANUARY 13, 1999

Primary sulphides occur both as micro-inclusions in major silicate and oxide phases and as individual grains in spinel lherzolite and pyroxenite xenoliths from Qilin, southeast China. Most of the lherzolite-hosted sulphide inclusions, typically 20–50 µm across, occur as isolated spheres or spheroids; host grains are olivine, clinopyroxene and orthopyroxene, but not spinel. In contrast, sulphide inclusions in pyroxenite are mostly 20–80 µm across and are almost exclusively hosted by clinopyroxene and spinel. These sulphide inclusions are typically multifaceted polygons, with their shapes epitaxially controlled by the host minerals. Isolated sulphide grains occur only in pyroxenite; they are up to 500 µm across, show evidence of deformation and are spatially associated with spinel. Lherzolite-hosted sulphide grains are polyphase assemblages that consist of pentlandite ± chalcopyrite ± Ni-poor monosulphide solid solution (mss1) ± Ni-rich monosulphide solid solution (mss2) ± cubanite ± heazlewoodite ± millerite ± bornite. Pyroxenite-hosted sulphide grains are pyrrhotite with minor chalcopyrite. All assemblages are likely to be the low-T (≤300°C) re-equilibrated products of high-T monosulphide solid solutions (MSS). The bulk compositions of these sulphide grains, estimated using proton microprobe analysis, show no consistent differences between the inclusion suites and intergranular sulphide grains, either in spinel lherzolite or pyroxenite samples. Average values of 111 proton microprobe analyses reveal that the lherzolite-hosted sulphides are rich in Ni (21%), Cu (<9%), Se (110 ppm) and platinum group elements (PGE) (≤30 ppm) but poor in Fe (37%) compared with the pyroxenite-hosted sulphides (Ni 1.4%, Cu <4%, Se 35 ppm, PGE absent, Fe 61.5%). Other trace elements (Co, Zn, As, Mo, Ag, Sn, Sb, Te and Pb) show no significant difference between

the two suites. Lherzolite-hosted sulphides are inferred to be derived from immiscible sulphide melts trapped in residual mantle during partial melting. The sulphide melts had themselves undergone MSS fractionation before their incorporation into the depleted mantle rocks. In contrast, pyroxenite-hosted sulphides were produced by sulphur saturation during the crystallization of mafic magmas intruded into lherzolitic mantle.

KEY WORDS: mantle sulphides; sulphide geochemistry; southeast China mantle; lherzolite sulphides; pyroxenite sulphides

INTRODUCTION

Sulphide minerals are common in mantle rocks and are likely to control the platinum group element (PGE), siderophile and chalcophile element budget of mantle rocks and their behaviour during melting, but little is known about the origin of mantle sulphides. Sulphide minerals potentially carry useful information about the mantle's composition and evolution as well as Re/Os isotopic systematics, which cannot be obtained by the study of silicate minerals. Petrogenetic studies of mantle sulphides ultimately may also help us better understand the genesis of base-metal sulphide deposits and PGE

* Present address: Phelps Dodge Australasia Inc., Level 15, 323 Castle-reagh Street, Sydney, N.S.W. 2000, Australia

† Corresponding author. Telephone: +61-2-9850-8362. Fax: +61-2-9850-8943. e-mail: sue.oreilly@mq.edu.au

mineralization associated with mafic-ultramafic intrusions.

Far more attention has been paid to immiscible sulphides in magmas (especially basaltic). Studies of mantle sulphide minerals are scarce. Samples of primary mantle sulphide minerals may be obtained from: (1) ultramafic xenoliths entrained in basaltic and kimberlitic rocks (e.g. Meyer & Brookins, 1971; Desborough & Czamanske, 1973; Frick, 1973; Vakhrushev & Sobolev, 1973; Bishop *et al.*, 1975; De Waal & Calk, 1975; Meyer & Boctor, 1975; Distler *et al.*, 1987; Mitchell & Keays, 1981; Lorand & Conqu  r  , 1983; Dromgoole & Pasteris, 1987; Fleet & Stone, 1990; Szab   & Bodnar, 1995); (2) inclusions in mantle-derived megacrysts and macrocrysts such as clinopyroxene, garnet and diamond (e.g. Peterson & Francis, 1977; Gurney *et al.*, 1984; Andersen *et al.*, 1987; Fleet & Stone, 1990; Rudnick *et al.*, 1993; Deines & Harris, 1995; Bulanova *et al.*, 1996); (3) tectonically exposed ultramafic sequences derived from the upper mantle (e.g. Lorand, 1989, 1991). Experimentally determined phase equilibria for sulphide and sulphide-silicate-oxide systems (Kullerud *et al.*, 1969; Craig, 1973; Misra & Fleet, 1973; Fleet & Pan, 1994; Karup-M  ller & Makovicky, 1995) carried out at atmospheric pressure can be applied directly to upper-mantle conditions because pressure changes the phase boundaries by <2  C/kbar (Bell *et al.*, 1964; Usselman, 1975). We report the mineralogy and characteristics of major and trace element compositions of sulphides in mantle xenoliths from Qilin in southeastern China, and discuss their origin and implications for some aspects of mantle processes based on the phase equilibria established by the above-mentioned experiments.

GEOLOGICAL CONTEXT AND SAMPLES

Basaltic rocks form a N-S trending Cenozoic volcanic belt in eastern China. At Qilin, they form a basaltic volcanic pipe that cuts Mesozoic granitic bodies (Fig. 1). Mantle xenolith samples of Phanerozoic subcontinental mantle are abundant in the Qilin volcanic pipe and include both peridotite and pyroxenite varieties (Xu *et al.*, 1996). Lherzolite accounts for >90% of all the mantle-derived xenoliths at this locality.

The peridotite xenoliths at Qilin represent mantle wall rocks and are spinel lherzolite with minor harzburgite. Most of them show porphyroclastic to equigranular textures. Grain sizes vary from 0.5 to 5 mm. The major phases are olivine, orthopyroxene, clinopyroxene and spinel. Amphibole and rare carbonate reflect mantle metasomatism. Olivine grains are either small or are porphyroclasts showing kink bands. Both fall into a compositional range Fo₈₉₋₉₁ (Table 1), a characteristic of

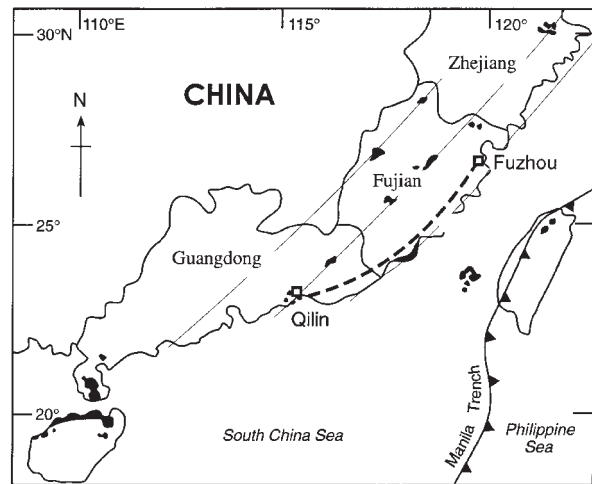


Fig. 1. Cenozoic basalts along regional faults in southeast China (filled areas). Qilin is located in the Puning County of Guangdong Province [adapted from Xu *et al.* (1996)].

Table 1: Observed sulphide mineral assemblages in spinel lherzolite xenoliths

Assemblage	Type	pn	mss1	mss2	chp	py	others
<i>3-phase</i>							
1	e	+	+	+			
2	e	+	+		+		
3	i	+			+		+ hz
4	i			+	+	+	
<i>2-phase</i>							
5	e	+	+				
6	e	+		+			
7	e		+	+			
8	e		+				+ cb
9	e			+	+		
10	e, i	+			+		
11	i						++ mi, bo
12	i	+					+ hz
<i>1-phase</i>							
13	e, i	+					
14	e, i				+		
15	i						+ hz

e, enclosed sulphide; i, intergranular sulphide; pn, pentlandite; mss1, low-Ni monosulphide solid solution; mss2, high-Ni monosulphide solid solution; chp, chalcopyrite; py, pyrite; cb, cubanite; mi, millerite; bo, bornite; hz, heazlewoodite.

the Cr-diopside suite of mantle xenoliths [‘Group I’ of Frey & Prinz (1978)]. Orthopyroxene is the second major phase in abundance and shows deformation to various

degrees; its composition is typically in the range of $\text{En}_{86-9-91-5} \text{Fs}_{7-2-11-6} \text{Wo}_{1-0-1-5}$ (Table 1). Clinopyroxene is third in abundance (Table 1). It occurs as bright green grains (in hand specimen) that are $\text{En}_{54-5-60} \text{Fs}_{2-9-6-2} \text{Wo}_{33-8-42-4}$. Spinel contains up to 30.5 wt % Cr_2O_3 and are commonly associated with Cr-diopside. The abundance and trace-element patterns of clinopyroxene and the magnesian composition of the major silicate minerals indicate that the Qilin lherzolites are moderately depleted residues after <10% of mantle (Xu *et al.*, 1999). The compositions of sulphide-bearing silicate minerals resemble those of sulphide-barren ones.

The pyroxenite xenoliths are mainly clinopyroxenite or websterite. Both contain spinel \pm garnet and, rarely, amphibole (Xu *et al.*, 1996). The garnet content of clinopyroxenite may reach 40 vol. % by volume (Zhao, 1985; Xu *et al.*, 1996). Pyroxene grains may be up to 5 mm across. These pyroxenite xenoliths are typical of the metapyroxenite series in the Al-augite xenolith suite recognized by Griffin *et al.* (1984) and O'Reilly & Griffin (1987) ['Group II' of Frey & Prinz (1978)]. They show extensive exsolution of orthopyroxene and garnet from clinopyroxene, and porphyroblastic to granoblastic textures. These features suggest that the xenoliths were metamorphosed within the mantle. The xenoliths show *mg*-number of 83–86, Al_2O_3 of 12.7–17.5 wt %, TiO_2 < 1.06 wt % and bimodal CaO features (14.9–15.8 wt % for clinopyroxenite and ~9.4 wt % for websterite; Zhao, 1985). These resemble those of the Al-augite suite of pyroxenite xenoliths in western Victoria, Australia (Griffin *et al.*, 1984, 1988). Garnet and orthopyroxene vary little in compositions. However, both clinopyroxene and spinel show a bimodal distribution of *mg*-number values. Sulphide minerals are associated only with the low-*mg*-number group (Fig. 2).

OCCURRENCE OF SULPHIDE MINERALS

Of 22 lherzolites and 26 pyroxenites from Qilin, SE China, eight lherzolites and nine pyroxenites contain sulphide minerals. The Qilin xenoliths show a range of microstructures similar to those reported earlier (e.g. Dromgoole & Pasteris, 1987; Szabó & Bodnar, 1995). However, no obvious correlations between rock microstructure and the sulphide mineral occurrence are seen in the Qilin suite. Most sulphide minerals occur either interstitial to the major silicate and oxide minerals or are enclosed completely as micro-inclusions within these phases and rarely as cross-cutting veins. These veins are obviously of secondary origin and were not studied.

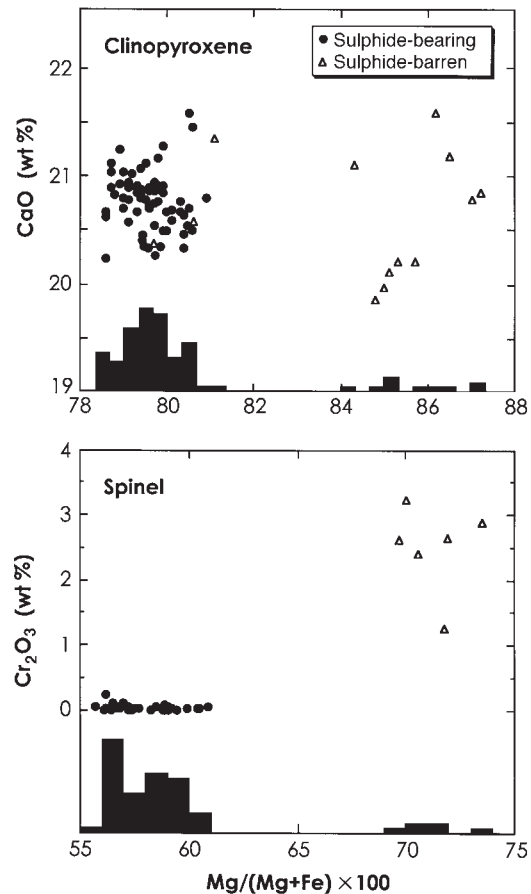


Fig. 2. Variations of *mg*-number vs CaO and Cr_2O_3 contents in clinopyroxene and spinel in the pyroxenite xenoliths. The bimodal distributions of *mg*-number for both phases are shown by the histogram inserts which are constructed based on 76 sulphide-bearing pyroxenes and 55 sulphide-bearing spinels out of a total nine rock samples. The plotted sulphide-barren minerals are mineral compositions averaged from more than four separate grains in each individual rock sample (Xu *et al.*, 1996).

Sulphide minerals in lherzolite samples

In lherzolite xenoliths, sulphide mineral inclusions are hosted by olivine, clinopyroxene and orthopyroxene, but not spinel or garnet if present. Most sulphide mineral inclusions are isolated spheres or spheroids ranging from 20 to 40 μm in diameter. At high scanning electron microscope magnifications, some of these inclusions exhibit polygonal cross-sections with straight contacts, a habit which may reflect entrapment. Sulphide mineral spheres, <10 μm , also decorate healed fractures in silicate grains. Some small sulphide mineral spheres appear to radiate out along fractures in the host grain from inclusions. Other trails of small sulphide mineral spheres appear to intersect larger sulphide mineral inclusions in the host mineral. Both types of trails may once have been sulphide droplets trapped along silicate sub-grain

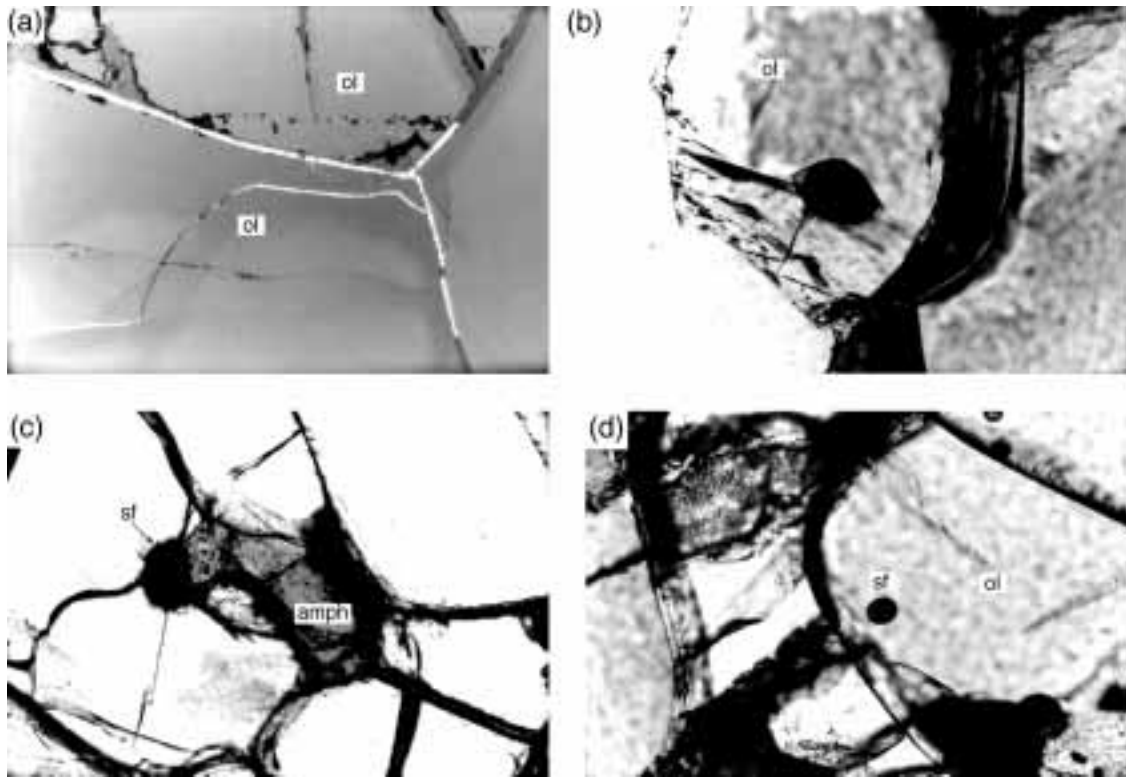


Fig. 3. Sulphide in spinel lherzolites. (a) Intergranular sulphide strips, $\sim 10\ \mu\text{m}$ thick, between olivine grains; (b) a large primary sulphide inclusion ($\text{MSS} \pm \text{L}$) that consists of re-equilibrated pentlandite (light grey) and Ni-rich monosulphide (mss2; dark grey) in olivine with intersecting fractures; (c) intergranular sulphide bleb adjacent to amphibole; (d) a primary sulphide inclusion ($\text{MSS} \pm \text{L}$) in olivine, with recognizable individual re-equilibrated phases, pentlandite in the margin and two monosulphides (mss1 and mss2) in the centre. Field of view is $0.85\ \text{mm}$ for (a) or $0.6\ \text{mm}$ for (b), (c) and (d).

boundaries, controlled by the cleavage or slip planes of the silicate host mineral (Frick, 1973). If an original fracture was completely annealed, the sulphide droplets may have become discrete small inclusions (Andersen *et al.*, 1987). Discrete, matrix sulphide mineral grains are as abundant as inclusions in spinel lherzolite minerals. The former are scattered throughout the rocks. They occur as small irregular blebs ($10\text{--}30\ \mu\text{m}$), as curved strips along grain contacts, or as subhedral grains at 120° triple junctions between mineral grains (Fig. 3). The last form suggests a post-deformation textural equilibrium with the silicate minerals, indicating that such sulphide grains were present during plastic deformation of the mantle rocks.

Amphibole-bearing spinel lherzolite sample Q9335 displays sulphide mineral grain intergrown with amphibole. This association may reflect mantle metasomatism of the subcontinental mantle at Qilin (Xu *et al.*, 1996).

Lherzolite xenoliths commonly contain pentlandite (pn), chalcopyrite (chp), Ni-poor monosulphide solid solution (mss1) and Ni-rich monosulphide solid solution (mss2; Fig. 5). Less common minerals are cubanite (cb) [no distinction is made between cubanite and isocubanite

in this paper, because of the lack of structural information], heazlewoodite (hz), millerite (mi) and bornite (br). Individual sulphide phases generally can be recognized by their reflectivity and colour tones. The microscopic features for common phases are: pn—pinkish yellow; chp—bright more saturated yellow; mss1—pink to pinkish grey; mss2—yellowish pink. The complexity of the sulphide assemblages in lherzolite xenoliths is summarized in Table 1. Pentlandite occurs in more than half of the total sulphide grains analysed, followed by chalcopyrite and monosulphide solid solutions. Chalcopyrite occurs as thin rims surrounding the Ni-Fe sulphide minerals that make up the grain core, in which exsolution textures composed of mss1 and mss2 are typically present. Pentlandite invariably occurs as large individual grains in the sulphide assemblage.

Sulphide minerals in pyroxenite samples

Sulphide mineral inclusions in pyroxenite xenoliths are almost exclusively hosted by clinopyroxene and spinel, even if garnet and orthopyroxene make up most of the

mode. In samples QL3 and QL22, however, spinel is the only phase that contains sulphide inclusions. Sample Q9324 is the only pyroxenite xenolith that contains sulphide mineral inclusions within orthopyroxene. This is in contrast to the findings of De Waal & Calk (1975), who described sulphide minerals as inclusions within clinopyroxene, garnet and orthopyroxene, but not in spinel. The diameters of sulphide mineral inclusions vary from $<5\ \mu\text{m}$ to $>200\ \mu\text{m}$ but most are 20–80 μm . The cross-sections of the sulphide mineral inclusions vary from spheres, elongated rods and squares to multifaceted polygons that reflect the lattice symmetry of the host pyroxene or spinel. The distribution of multiple sulphide inclusions within a single grain is also controlled by the structure of their host minerals, which creates a distinctive grid arrangement (Fig. 4b). Most sulphide inclusions appear to be isolated within the host grain and show no visible cross-cutting fractures. Sulphide grains are oxidized where major fractures cut them. Such regions are partly or wholly converted to magnetite. However, some primary oxide minerals appear to coexist with sulphide within a single spherical inclusion; these oxide minerals may have formed by unmixing of an original oxysulphide liquid (Fig. 4f). Matrix sulphide mineral grains are generally large, up to 500 μm across with shapes that vary from rounded blebs with anhedral or straight grain contacts to deformed and elongated grains. Some grains are partially oxidized or altered. Large sulphide mineral grains commonly are adjacent to spinel, which suggests that two mineral types are genetically related. In some samples, large sulphide mineral grains are abundant in parts of the rock but absent in other parts.

The sulphide mineral assemblage in the pyroxenite xenoliths consists predominantly of pyrrhotite and minor chalcopyrite regardless of textural occurrence (Table 3, below). Chalcopyrite occurs either as thin lamellae or as thin rims that surround pyrrhotite grains. Chalcopyrite in a single sulphide inclusion is generally 5 vol. %, but ranges to 25 vol. %. Rarely, pentlandite and millerite are found in the pyroxenite-hosted sulphide mineral inclusions, as the result of exsolution or alteration (e.g. in samples QL22 and Q9324, respectively; see Table 3, below). Most large pyrite grains in pyroxenite samples QL2, QL3 and QL21 are typically associated with strings of small fluid inclusions that occur along intersecting fractures in major minerals. A few large pyrite grains replace part of pyrrhotite grains.

MINERALOGY AND CHEMISTRY

Analytical techniques

Major element contents of minerals were analysed on the CAMECA Camebax SX50 electron microprobe

(EMP) at the School of Earth Sciences, Macquarie University. Silicate analyses were performed with 15 kV accelerating voltage and a 20 nA beam current. Counting times were 20 s. A combination of natural and synthetic minerals was used for standard calibration and the matrix corrections were carried out using the Cameca PAP correction routine. Counting time for Ni was 40 s (30 s peak, 10 s background) to lower the detection limit for this element. Analyses of sulphide mineral grains were performed at 20 kV accelerating voltage to enhance signals. The elements in routine analysis of sulphide minerals were Fe, Co, Ni, Cu, Zn, S and O.

Trace element analyses were obtained using the HIAF proton microprobe at CSIRO Exploration and Mining (North Ryde). The high-energy proton beam from a tandem electrostatic accelerator is focused onto the sample by an electrostatic lens. Secondary X-rays pass through a 300 μm Al filter, which attenuates X-rays of major elements. Remaining X-rays are collected by an Si(Li) energy-dispersive detector and concentrations determined as described by Ryan *et al.* (1990). The typical size of the beam spot on the sample is around 30 μm in diameter and the beam current is 10–15 nA. The analysed volume is $\sim 35\ \mu\text{m}$ deep. In the present study, the polyphase nature of most sulphide mineral grains made it impossible to obtain X-ray signals for a single phase. The raw data were normalized to monosulphide ($\text{FeS} + \text{NiS} + \text{CuS}$) = 100%, so that concentrations for Zn, As, Se, Mo, Ru, Rh, Pd, Ag, Sn, Sb, Te, and Pb have uncertainties of the same magnitude as those for Fe, Ni and Cu, because of deviation from perfect stoichiometry. The analytical accuracy of these concentrations is believed to be better than $\pm 10\%$ for most of the elements reported in this paper. The uncertainties given in Tables 4 and 5 (see below) are derived from counting statistics and the minimum detection limits (MDL) are given at the 99% confidence level.

Chemical composition of sulphide minerals

Pentlandite

Pentlandite varies widely in its Ni contents, most of which range from 33 to 44 wt %. Ni/(Ni + Fe) ratios of the pentlandite are normally distributed in the range of 55–65, which, although similar to that reported by Szabó & Bodnar (1995), is slightly more Ni rich (Fig. 6a). Pentlandite in inclusions is the same composition as matrix pentlandite. Some analyses show lower Ni contents, coupled with lower metal/sulphur ratio (M/S), which reflect mixture of pn + mss. Co contents are mostly between 0.2 and 0.8 wt %, with some up to 1.6 wt %. Most Cu contents are <1.8 wt % but a few values scatter up to 6.9 wt %. High Cu analyses may be due to contamination by submicroscopic inclusions of

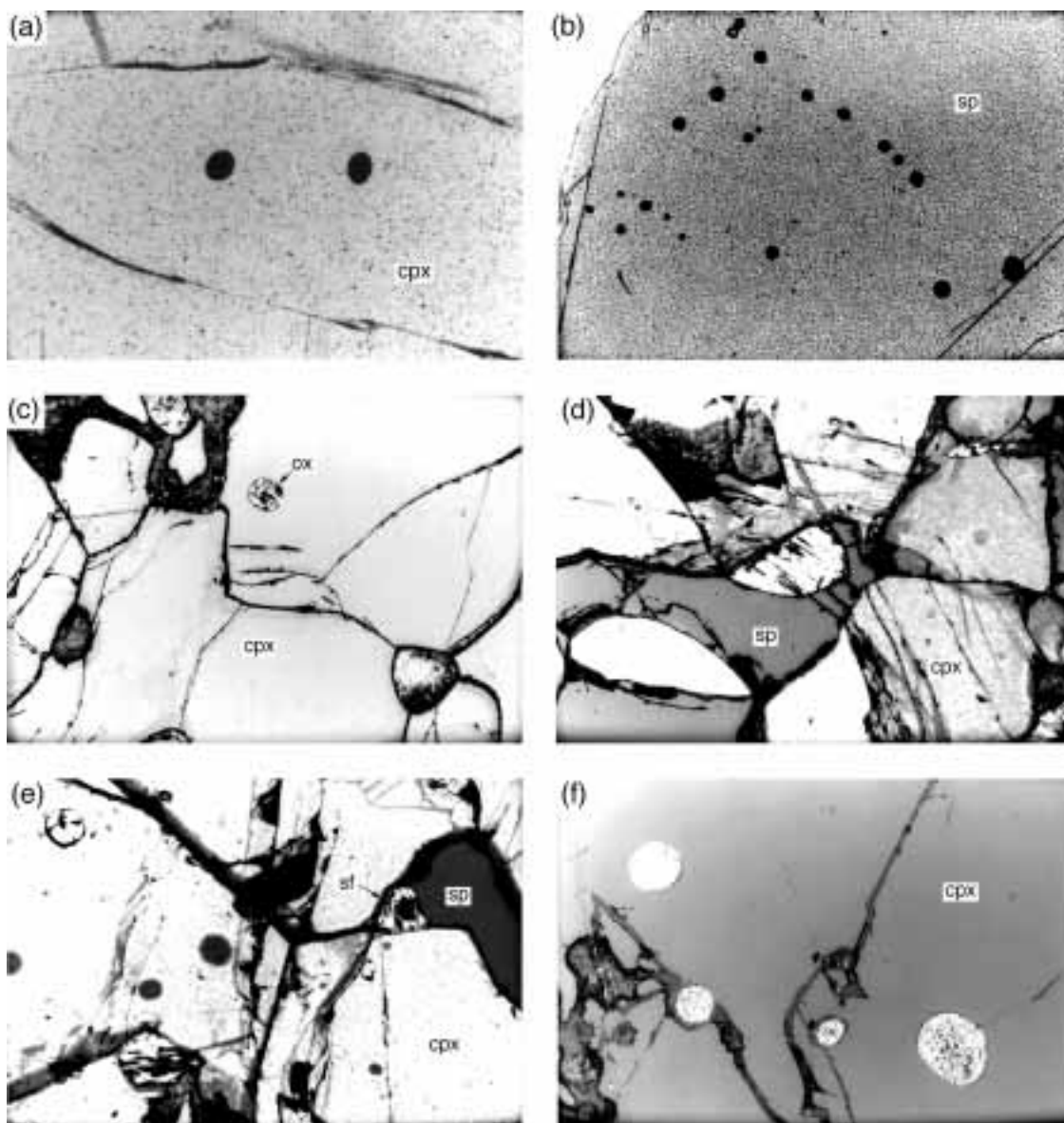


Fig. 4. Sulphide occurrences in pyroxenites. (a) Approximately 60 μm , spheroid sulphide inclusions (mainly pyrrhotite) in clinopyroxene; (b) sulphide inclusions forming right-angled grid in spinel, with the largest dimension of a single grain measuring 80 μm ; (c) enclosed and intergranular oxide grains in and between clinopyroxenes, with the enclosed grain measuring $\sim 200 \mu\text{m}$; (d) a large intergranular sulphide grain, $>1 \text{ mm}$, adjacent to spinel; (e) a spherical sulphide inclusion in clinopyroxene and intergranular sulphide at a 120° triple junction (the rounded grey areas are shadows of sulphide inclusions at depth); (f) inclusion grains in clinopyroxene showing sulphide-oxide unmixing, with the largest grain measuring approximately $80 \mu\text{m} \times 100 \mu\text{m}$.

chalcopyrite. Zn is generally $<0.05 \text{ wt } \%$. The ubiquitous presence of oxygen in the pentlandite is noteworthy; oxygen contents cluster around $0.5 \text{ wt } \%$ with some values as high as $3 \text{ wt } \%$. However, these values represent $<5\%$ atomic substitution of sulphur by oxygen.

Monosulphide solid solutions

The abbreviations mss1 and mss2 are used for monosulphide solid solutions we found in the sulphide mineral

grains. These terms correspond to the low- T phases mss1 and mss2 of Craig (1973). The abbreviation MSS describes inferred primary mantle monosulphide solid solutions. This is equivalent to the experimentally derived high- T MSS of Kullerud *et al.* (1969).

Nickeliferous monosulphide solid solutions form parts of sulphide mineral inclusions only in peridotite samples. Their variable compositions suggest that they are solid solutions, with one being Ni poor (mss1) and the other

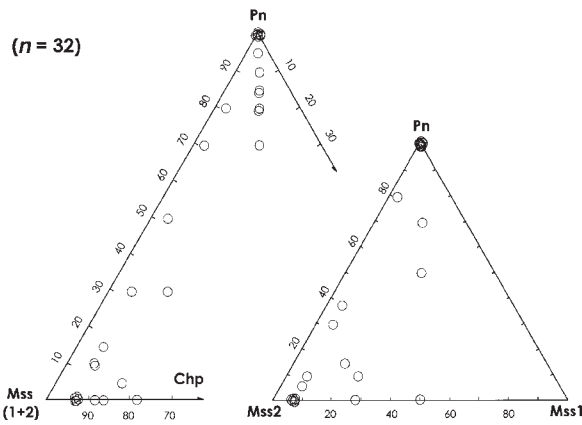


Fig. 5. The proportions of major phases in each single sulphide inclusion found in peridotites. The inclusions are hosted by olivine, clinopyroxene and orthopyroxene. The total number of inclusions is 32. Pn, pentlandite; MSS, monosulphide solid solution; Chp, chalcopyrite.

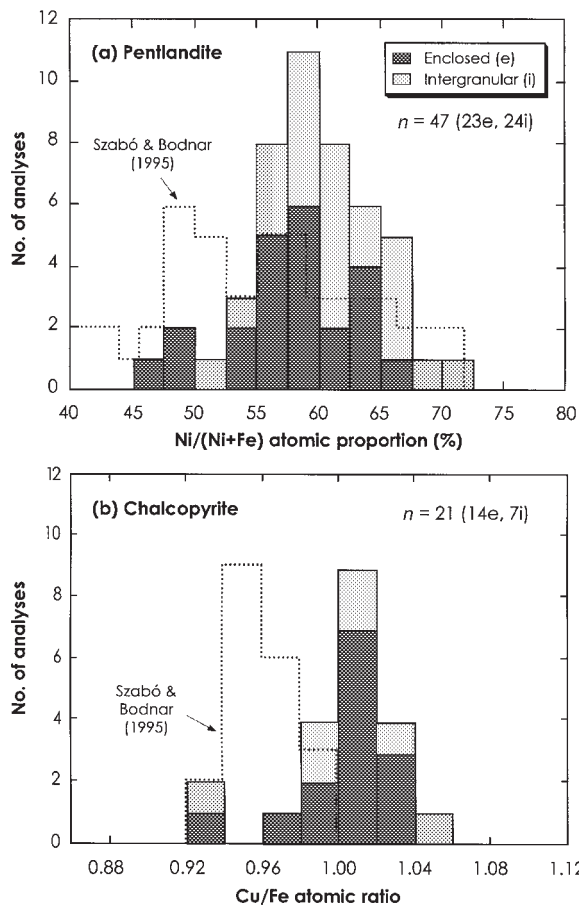


Fig. 6. Stacked histogram showing (a) Ni/(Ni + Fe) atomic ratios of pentlandite and (b) Cu/Fe atomic ratios of chalcopyrites occurring in the multi-phase sulphide assemblages in spinel lherzolites. The dotted line represents data from the peridotites of the Nógrád–Gömör Volcanic Field in eastern Europe (Szabó & Bodnar, 1995)

being Ni rich (mss2) (Fig. 7, Table 2). A lherzolite-hosted monosulphide with as little as 3 wt % Ni (e.g. grain Q9321/s11.2e) is treated as mss1 in this study although 5 wt % Ni has been accepted as the upper limit of pyrrhotite composition (e.g. Dromgoole & Pasteris, 1987; Szabó & Bodnar, 1995). Based on 20 examples we studied, 10 wt % Ni is probably the compositional boundary between the two types of monosulphide solid solution. The best constraint for this division comes from a zoned mss1 grain in sample Q9321, in which Ni contents vary from 25.2 wt % at the centre to 9.95 wt % at the rim (Table 2). The M/S ratios of mss1 are 0.8–0.9, corresponding to a metal deficit of 0.1–0.2 in the monosulphide structure, making it ‘pyrrhotite like’. The M/S ratios of mss2 are 1.0–1.1. The Ni-poor mss1 seems to correlate better with the monoclinic sulphide Fe_7S_8 , whereas the Ni-rich mss2 shows significantly higher M/S ratios (Fig. 7); this contrasts with Szabó & Bodnar (1995), who found that the lherzolite-hosted MSS is closer to hexagonal Fe_9S_{10} .

Chalcopyrite

Chalcopyrite is the most common Cu-rich mineral in the Qilin xenolith suite. Lherzolite-hosted chalcopyrite shows compositions close to the $CuFeS_2$ stoichiometry in contrast to the Cu-deficient chalcopyrite reported by Szabó & Bodnar (1995) (Fig. 6b). There is no difference in composition between chalcopyrite in inclusions and matrix grains. Ni contents of the chalcopyrite are <0.8 wt %. Chalcopyrite also occurs in the pyroxenite-hosted sulphide mineral assemblages but quantitative analyses were obtained only for a few grains, because of their generally small size. The compositions of pyroxenite-hosted chalcopyrite resemble those of lherzolite-hosted ones, with normal $CuFeS_2$ stoichiometry.

Pyrrhotite

Here pyrrhotite describes Ni-poor monosulphide minerals. Five weight percent Ni is generally regarded to be the maximum Ni solubility in the pyrrhotite structure (e.g. Cabri, 1973). Pyrrhotite is the principal constituent of sulphide mineral grains in the pyroxenite xenoliths. Most Ni contents of pyrrhotite are <1 wt %, but some range to 4 wt %. Most Co and Cu contents are <0.3 wt % and 0.1 wt %, respectively. Compositions of pyrrhotite inclusions in clinopyroxene grains resemble those included within spinel; this suggests equilibrium between sulphide and host minerals. Matrix pyrrhotite grains show M/S ratios significantly lower than their counterparts that occur as inclusions. The former have typically lower Fe contents. However, the minor element contents of matrix pyrrhotite appear consistent with those that occur as inclusions. Thus, the low M/S ratios probably result from crustal alteration rather than Fe loss during mantle metasomatism (Szabó & Bodnar, 1995).

Table 2: Representative electron microprobe analyses of individual phases in the polyphase sulphide assemblages hosted by spinel lherzolites

Phase:	Pentlandite (pn)									
Sample no.:	Q9304			Q9321				Q9329		
Sulphide label:*	s1.3e	s1.5i	s3.3i	s2e	s12.2e	s16.1e	s22.2e	s5.3i	s4.2e	s1.1i
Assemblage:†	10	13	3	13	2	13	5	13	5	13
<i>Concentration (wt %)</i>										
Fe	32.36	24.43	23.56	22.06	27.15	23.28	27.27	27.53	26.92	20.39
Co	0.53	0.70	0.54	0.66	0.63	0.69	0.55	0.51	0.86	1.64
Ni	29.52	39.47	39.95	41.45	36.66	40.37	36.22	36.60	37.23	43.34
Cu	2.77	1.11	0.09	0.43	0.61	0.01	0.40	0.04	0.21	0.08
Zn	0.05	0.00	0.00	0.01	0.00	0.00	0.00	0.00	0.02	0.00
S	32.61	33.56	33.14	33.47	33.46	33.58	33.47	33.33	33.40	32.90
O	1.06	0.40	0.83	0.35	0.31	0.38	0.44	0.35	0.49	0.44
Total	98.90	99.67	98.10	98.44	98.82	98.31	98.35	98.37	99.13	98.80
M/S ratio‡	1.12	1.09	1.08	1.07	1.08	1.07	1.07	1.08	1.09	1.10
100O/(S + O)§	6.1	2.3	4.8	2.1	1.8	2.2	2.6	2.1	2.8	2.6

Phase:	Pentlandite (pn)									
Sample no.:	Q9335						Q9342	Q9345	QL27	
Sulphide label:	s1.4e	s6.2e	s8.3e	s9.3e	s10.1e	s10.2e	s1.5i	s1.4e	s1.2i	s4.1e
Assemblage:	10	10	6	2	13	13	10	10	13	10
<i>Concentration (wt %)</i>										
Fe	27.65	23.62	29.53	27.85	27.31	26.80	21.22	24.49	26.67	33.29
Co	0.39	0.44	0.45	0.59	0.40	0.24	0.80	0.39	0.51	0.37
Ni	37.73	41.81	35.95	37.00	38.08	37.81	43.68	40.46	37.82	29.65
Cu	0.40	0.48	0.09	0.52	0.27	0.42	0.81	0.39	0.79	0.15
Zn	0.00	0.00	0.00	0.01	0.00	0.00	0.01	0.02	0.06	0.03
S	33.09	32.87	33.39	33.37	32.83	32.68	32.82	33.26	33.00	33.98
O	0.34	0.68	0.44	0.37	0.47	1.03	0.40	0.49	0.50	2.03
Total	99.58	99.89	99.84	99.70	99.36	98.97	99.73	99.50	99.35	99.50
M/S ratio	1.11	1.12	1.10	1.10	1.12	1.11	1.12	1.10	1.11	1.05
100O/(S + O)	2.0	4.0	2.5	2.1	2.8	6.0	2.4	2.9	3.0	10.7

Phase:	(pn)	Ni-poor mss (mss1)								
Sample no.:	QI27	Q9321								
Sulphide label:	s7.4e	s1.4e/rim	s1.5e/core	s4.3e	s5.3e	s11.2e	s12.3e	s13.1e	s13.3e	s21.3e
Assemblage:	10	7	7	5	7	5	2	1	1	5
<i>Concentration (wt %)</i>										
Fe	35.27	48.70	30.79	47.84	45.70	55.96	48.11	44.72	51.97	40.13
Co	0.36	0.14	0.49	0.15	0.21	0.03	0.09	0.38	0.15	0.39
Ni	28.74	9.95	25.20	10.59	13.96	3.09	10.34	14.85	6.92	19.31
Cu	0.09	0.04	0.05	0.07	0.03	0.01	0.07	0.07	0.03	0.02
Zn	0.08	0.00	0.02	0.01	0.00	0.02	0.03	0.00	0.03	0.02
S	34.20	39.43	41.46	39.59	38.57	39.03	39.20	38.49	39.00	38.97
O	1.41	0.38	0.42	0.34	0.40	0.39	0.40	0.43	0.38	0.28
Total	100.15	98.65	98.42	98.59	98.88	98.52	98.24	98.93	98.46	99.12
M/S ratio	1.06	0.85	0.77	0.84	0.88	0.87	0.85	0.88	0.86	0.87
100O/(S + O)	7.6	1.9	2.0	1.7	2.1	2.0	2.0	2.2	1.9	1.4

Phase:	Ni-poor mss (mss1)						Ni-rich mss (mss2)			
Sample no.:	Q9329		Q9335	Q9345		QL27	Q9321		Q9329	
Sulphide label:	s2.1e	s4.1e	s9.1e	s1.1e	s2.2e	s6.2e	s4.2e	s13.2e	s1e	s3i
Assemblage:	5	5	2	7	7	8	6	1	6	9

Concentration (wt %)

Fe	53.85	45.41	47.52	49.15	40.94	52.49	32.44	33.43	38.48	19.00
Co	0.07	0.17	0.13	0.10	0.58	0.07	0.39	0.21	0.32	1.64
Ni	4.31	12.46	11.67	9.23	20.84	5.74	31.12	22.48	21.21	35.93
Cu	0.17	0.11	0.00	0.06	0.06	0.15	0.17	6.90	2.13	6.89
Zn	0.00	0.01	0.00	0.01	0.00	0.02	0.03	0.00	0.00	0.07
S	39.31	39.46	38.91	38.46	37.68	39.47	35.96	34.72	36.30	32.45
O	0.24	0.40	0.34	0.51	0.35	0.74	0.33	0.40	0.73	2.21
Total	97.95	98.01	98.56	97.52	100.44	98.67	100.44	98.13	99.17	98.20
M/S ratio	0.85	0.84	0.87	0.87	0.94	0.85	1.05	1.01	0.96	1.08
100O/(S + O)	1.2	2.0	1.7	2.6	1.8	3.6	2.28	2.3	3.9	12.0

Phase:	Ni-rich mss (mss2)				Chalcopyrite (chp)					
Sample no.:	Q9335	Q9345	QL27		Q9304	Q9321	Q9329	Q9335	Q9342	QL27
Sulphide label:	s10i	s2.1i	s7.5e	s3.1i	s1.2e	s9e	s5i	s2.2e	s1.7e	s8.2i
Assemblage:	6	6	6	4	10	14	14	14	10	10

Concentration (wt %)

Fe	23.03	24.84	42.73	35.92	29.72	30.05	29.57	29.82	29.74	29.60
Co	0.78	0.61	0.28	0.44	0.00	0.00	0.03	0.00	0.01	0.00
Ni	35.99	33.00	18.58	27.83	0.79	0.45	0.29	0.40	0.34	0.46
Cu	3.78	6.52	0.12	0.07	33.16	31.84	34.44	34.05	33.68	33.66
Zn	0.01	0.00	0.02	0.00	0.00	0.01	0.02	0.03	0.01	0.01
S	32.50	33.13	36.10	34.29	34.61	35.45	34.45	34.80	34.35	34.59
O	3.05	0.70	0.55	0.79	0.49	0.69	0.32	0.84	0.38	1.66
Total	99.13	98.81	98.37	99.35	98.76	98.49	99.11	99.94	98.50	99.98
M/S ratio	1.08	1.08	0.97	1.05	0.99	0.95	1.00	0.99	1.00	0.99
100O/(S + O)	15.81	4.1	3.0	4.4	2.7	3.8	1.8	4.6	2.2	8.8

Phase	Bornite (bo)			Heazlewoodite (hz)		Cubanite (cb)		Millerite (mi)	
Sample no.:	Q9335	Q9304	Q9342		QL27	Q9335			
Sulphide label:	s4.5e	s2.1i	s1.1i	s2.3i	s6.1e	s4.3e			
Assemblage:	11	15	15	15	8	11			

Concentration (wt %)

Fe	13.30	3.11	2.99	1.23	38.67	1.27			
Co	0.03	0.12	0.08	0.09	0.07	0.40			
Ni	0.53	69.49	67.75	70.90	3.40	63.23			
Cu	58.48	0.42	2.26	1.26	19.79	0.35			
Zn	0.00	0.00	0.03	0.00	0.00	0.00			
S	27.84	27.36	27.20	26.74	36.61	35.32			
O	0.34	0.27	0.48	0.69	0.65	0.16			
Total	100.51	100.77	100.78	100.90	99.18	100.73			
M/S ratio	1.35	1.46	1.47	1.50	0.93	1.01			
100O/(S + O)	2.4	1.9	3.4	4.9	3.4	0.9			

*The letters e and i denote enclosed and intergranular types, respectively.

†The assemblage patterns are given in Table 2.

‡M/S ratio is total-metals/sulphur ratio.

§Atomic proportion of oxygen substituting sulphur.

Table 3: Representative electron microprobe analyses of individual phases in the sulphide grains hosted by pyroxenites

Phase:	Pyrrhotite (po)																							
	OL2				OL3				OL7				OL15											
Sample no.:	s1e-po	s11e-po	s13e-po	s26e-po	s27e-po	s35e-po	s36e-po	s37e-po	s5e-po	s8e-po	s7e-po	s9e-po	s10e-po	s11e-po	s4e-po	s2e-po	s4e-po	s7e-po	s10e-po	s11e-po	s9e-po	s12e-po		
Sulphide label:	po+chp po+chp																							
Intergrowth:																								
Concentration (wt %)																								
Fe	58-16	57-43	56-29	59-10	58-79	58-51	57-68	58-25	58-53	58-27	58-57	58-76	59-42	59-67	58-79	60-34	59-67	59-59	60-11	60-11	56-17	57-29	59-39	57-37
Co	0-16	0-45	0-23	0-00	0-08	0-00	0-67	0-19	0-00	0-04	0-19	0-00	0-05	0-40	0-60	0-00	0-02	0-00	0-00	0-00	0-22	0-16	0-16	0-11
Ni	0-48	1-89	0-50	0-31	0-51	0-29	0-95	0-45	0-27	0-26	0-86	0-36	0-25	1-17	1-03	0-29	0-75	0-38	0-21	0-46	0-84	0-65	0-50	0-59
Cu	0-04	0-00	0-01	0-04	0-06	0-02	0-05	0-06	0-09	0-07	0-05	0-04	0-04	0-00	0-07	0-03	0-12	0-06	0-12	0-04	0-07	0-06	0-07	0-07
Zn	0-01	0-04	0-07	0-00	0-00	0-01	0-00	0-00	0-01	0-00	0-04	0-06	0-03	0-03	0-00	0-03	0-03	0-01	0-02	0-02	0-00	0-00	0-01	0-03
S	38-70	38-36	41-07	38-49	38-36	38-43	38-47	38-49	39-17	38-65	38-60	39-20	39-36	38-35	38-71	38-71	38-68	38-27	38-53	38-48	40-01	40-94	38-66	40-84
O	0-49	0-20	0-38	0-32	0-37	0-18	0-57	0-34	0-28	0-42	0-66	0-65	0-55	0-62	0-50	0-67	0-58	0-59	0-50	0-71	1-19	0-90	0-85	0-85
Total	98-03	98-38	98-55	98-26	98-16	97-43	98-39	97-78	98-35	97-72	98-77	98-06	99-70	100-23	99-70	100-07	99-86	98-90	99-48	99-83	98-50	100-00	99-65	99-85
M/S ratio*	0-87	0-89	0-80	0-89	0-89	0-88	0-88	0-88	0-86	0-87	0-88	0-87	0-87	0-92	0-90	0-90	0-90	0-90	0-90	0-90	0-82	0-81	0-89	0-82
100O/(S + O)t	2-47	1-01	1-83	1-63	1-91	0-92	2-87	1-75	1-42	2-14	3-32	3-22	2-72	3-15	2-51	3-36	2-93	2-98	2-52	3-57	5-61	4-23	4-22	3-98
FeS mol %	98-91	96-26	98-77	99-44	98-97	99-51	0-98	0-99	99-42	99-40	98-57	98-36	99-47	97-57	97-33	99-50	98-61	99-29	99-51	99-21	98-13	98-59	98-85	98-75
NIS mol %	0-77	3-02	0-84	0-50	0-81	0-46	0-02	0-01	0-44	0-43	1-06	0-58	0-40	1-81	1-62	0-45	1-19	0-60	0-32	0-72	1-40	1-07	0-78	0-96
Host minerals (cpx and spjt)																								
FeSiO ₃ mol %	11-26	11-08	11-02	11-33	10-86	11-29	10-43	10-39		11-01	11-06	11-14	10-96	10-81	10-81	10-73		10-67	10-63	10-54	10-46	10-91		
NiSiO ₃ mol %	0-02	0-03	0-03	0-05	0-05	0-07	0-09	0-04		0-04	0-02	0-10	0-05	0-05	0-05	0-02		0-04	0-07	0-05	0-14	0-05		
mg-no.	0-79	0-79	0-79	0-79	0-80	0-79	0-81	0-81	0-56	0-80	0-79	0-79	0-80	0-80	0-80	0-80	0-57	0-80	0-80	0-80	0-80	0-80	0-38	0-58
K ₁ Ni-Fe. sul/cpx	5-25	12-44	2-76	1-26	1-97	0-72	2-25	16-48		1-22	7-11	0-65	0-86	4-46	3-89	2-17		1-66	0-51	1-51	1-07	2-60		

Phase:	Pyrrhotite (po)				Chalcopyrite (chp)				Pentlandite (pn)				Millerite(mi)			
	QL18	QL21	OL22	09355	QL2	09355	OL22	08324	QL22	08324	QL22	08324		09324		
Sample no.:	s18e-po	s19e-po	s27e-po	s38e-po	s40e-po	s7e-po	s8e-po	s9e-po	s1e-po	s2e-po	s36e-chp	s23i-chp	s2e-chp	s1i-chp	s1e-pn	s2i-mi
Sulphide label:	s18e-po	s19e-po	s27e-po	s38e-po	s40e-po	s7e-po	s8e-po	s9e-po	s1e-po	s2e-po	s36e-chp	s23i-chp	s2e-chp	s1i-chp	s1e-pn	s2i-mi
Intergrowth	po+pn		po+pn		po+pn		po+pn		po+pn		po+pn		po+pn		po+pn	
<i>Concentration (wt %)</i>																
Fe	57.12	57.53	57.14	57.20	57.55	56.38	57.65	57.70	55.58	57.34	30.27	29.78	26.81	26.81	33.74	1.79
Co	0.25	0.03	0.26	0.04	0.20	0.77	0.10	0.06	0.22	0.52	0.01	0.15	0.10	0.42	0.80	0.60
Ni	0.57	0.25	0.68	0.44	0.48	2.36	0.37	0.33	0.40	3.63	0.10	0.25	0.46	1.24	21.94	61.24
Cu	0.02	0.02	0.04	0.04	0.02	0.05	0.05	0.19	0.06	0.03	33.18	33.78	28.81	34.27	5.41	0.31
Zn	0.00	0.03	0.01	0.00	0.00	0.00	0.00	0.02	0.00	0.00	0.04	0.07	0.00	0.00	0.00	0.01
S	38.63	38.80	39.27	38.58	38.64	38.37	39.15	38.70	39.27	38.41	34.57	35.20	34.85	34.39	34.32	35.07
O	0.85	0.72	0.58	1.04	0.61	1.15	0.39	0.79	0.58	0.49	0.23	0.19	0.73	0.31	0.82	0.56
Total	97.45	97.37	98.00	97.33	97.50	99.08	97.71	97.79	96.41	100.42	98.40	98.42	97.83	97.43	97.03	99.58
M/S ratio*	0.86	0.86	0.85	0.86	0.86	0.89	0.85	0.86	0.83	0.92						
1000/(S + O)†	4.24	3.59	2.90	5.13	3.06	5.64	1.96	3.91	2.87	2.48	1.30	1.06	4.03	1.79	4.57	3.11
FeS mol %	98.62	99.52	98.40	99.15	98.87	94.92	99.17	99.08	0.99	93.51						
NiS mol %	0.94	0.40	1.12	0.73	0.78	3.78	0.60	0.54	0.01	5.63						
<i>Host minerals (cpx and sp)‡</i>																
FeSiO ₃ mol%	10.63	10.41	10.95	10.33	10.88		11.07			10.39						
NiSiO ₃ mol%	0.12	0.08	0.03	0.05	0.03		0.06			0.04						
mg-no.	0.80	0.81	0.80	0.81	0.80	0.59	0.79	0.56		0.81						
K ₂ Ni-Fe ₂ sulfepx	0.63	0.54	4.37	1.67	2.54		1.20			16.48						

*M/S ratio is total-metals/sulphur ratio.

†Atomic proportion of oxygen replacing sulphur.

‡The compositions of the host minerals are the averages of several individual analyses, typically 2–4.

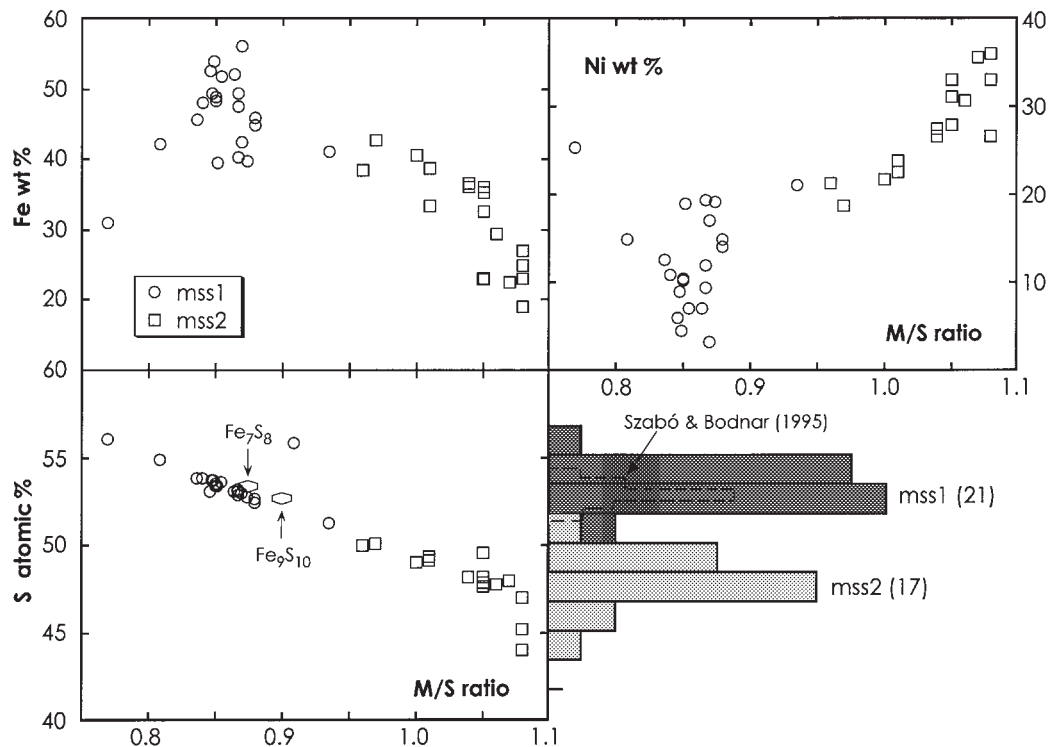


Fig. 7. Compositional characteristics of the two monosulphides (mss1, mss2) found in the enclosed multi-phase sulphide assemblages in spinel lherzolites. The theoretical monoclinic Fe_7S_8 and hexagonal Fe_9S_{10} sulphides are shown for comparison.

Minor phases

In lherzolite-hosted sulphide mineral grains, heazlewoodite contains up to 3.1 wt % Fe and 2.3 wt % Cu. Millerite and cubanite are close to stoichiometric compositions, and the latter contains 3.4 wt % Ni based on one quantitative analysis. Bornite was found in one sulphide mineral grain in spinel lherzolite sample Q9335.

Bulk composition

Estimating the bulk composition of primary mantle sulphide minerals has been a challenging task (e.g. De Waal & Calk, 1975; Dromgoole & Pasteris, 1987; Szabó & Bodnar, 1995). We employed the proton microprobe (PMP), which allows rapid, accurate and non-destructive *in situ* analysis of micro-volume samples. Unlike the EMP, which analyses only to depths of a few microns, the proton beam samples to depths of at least 30 μm in sulphide matrices. Not only can it analyse the whole volume of a multi-phase sulphide assemblage by adjusting the size of the proton beam, it also provides data for minor and trace elements at ppm levels. Compared with EMP-base reconstituted bulk compositions, PMP-derived bulk compositions of sulphide grains exhibit smaller standard deviations for Fe and Ni (Tables 4 and 5). The effect is especially clear for Ni and Cu, for which large

errors can be introduced by overestimation of pentlandite and underestimation of chalcopyrite. However, the Cu contents above 10% we obtained by PMP reflect oversampling of chalcopyrite in grains <30 μm thick.

Elements determined above PMP detection limits (MDL) are grouped as: (1) major transition elements, Fe, Co, Ni, Cu and Zn; (2) non-metallic elements, Se and As; (3) platinum group elements, Ru, Rh and Pd; (4) other heavy elements, Mo, Ag, Sn, Sb, Te and Pb. The content of any element may vary significantly between sulphide minerals from inclusions and matrix sulphide mineral grains in both lherzolite and pyroxenite samples (Fig. 8). In fact, the trace element data reveal more similarities than differences for the two textural types of sulphide mineral grains.

Sulphide grains in lherzolite samples average 37 wt % Fe, but range between 19.6 and 51.3 wt %. This range is similar to those found in earlier studies of lherzolite sulphide minerals (Dromgoole & Pasteris, 1987; Szabó & Bodnar, 1995). Pyroxenite-hosted sulphide grains average 61.5 wt % and range between 56.8 and 63.4 wt %. This is consistent with the dominance of pyrrhotite in the assemblage.

Most Ni contents of sulphide grains from lherzolite samples range from 12 to 30 wt %, which is also broadly consistent with the studies of Dromgoole & Pasteris

Table 4: Proton microprobe analyses of sulphide grains in spinel ilmenite

Sulphide	Host	Fe %	Ni %	Cu %	Zn	As	Se	Mo	Ru	Rh	Pd	Ag	Sn	Sb	Te	Pb
<i>Enclosed (23)</i>																
QL27-4e	opx	35.6	21.7	7.4	<37	<10	157±16	<6	10±3	<6	19±4	10±4	20±6	<15	20±9	<27
Q9321-1e	opx	34.6	18.2	11.8	101±59	<10	113±6	8±3	6±3	<6	8±5	9±4	13±7	15±8	<18	22±16
Q9321-2e	cpx	38.2	16.5	9.9	<27	<8	112±8	18±5	<5	18±6	17±7	<6	29±13	52±17	68±22	<17
Q9321-3e	ol	48.3	15.6	0.7	170±92	<15	77±7	13±6	9±6	11±6	<5	14±23	31±15	31±18	33±22	<45
Q9321-5e	cpx	40.4	18.4	5.8	<22	23±13	101±14	11±8	27±10	<5	<5	26±12	30±24	77±30	79±35	47±32
Q9321-6e	cpx	43.6	13.0	7.9	<20	<7	74±23	11±13	22±15	29±17	36±19	38±22	28±42	<13	95±68	116±57
Q9321-9e	cpx	37.0	24.6	3.0	<170	<10	112±7	7±3	<6	<6	6±4	8±4	25±8	<13	<16	30±14
Q9321-10e	ol	31.4	12.7	20.5	<812	<9	79±6	<5	6±4	8±5	8±5	9±5	218±17	16±17	<18	<25
Q9321-11e	cpx	33.2	29.7	1.7	<160	<11	108±4	10±2	<6	<7	<7	<8	13±5	<14	<17	<30
Q9321-12e	opx	40.8	21.2	2.6	<185	<10	108±5	12±3	<6	8±3	—	8±4	16±6	<14	<18	<29
Q9321-13e	cpx	41.5	22.4	0.7	<31	<11	139±5	17±3	<6	<6	<7	<7	31±6	<13	18±10	<29
Q9321-14e	cpx	33.7	17.6	13.3	48±64	<11	86±5	7±3	<6	9±3	<6	12±4	<12	18±9	37±11	<28
Q9321-15e	cpx	47.3	16.5	0.8	80±69	22±26	48±29	<4	<4	23±20	54±21	95±29	56±54	93±60	<16	38±61
Q9321-18e	cpx	44.3	19.5	0.8	<60	<9	125±7	21±4	8±6	<5	10±4	16±5	19±11	21±11	<17	<23
Q9335-1e	ol	35.3	16.6	12.8	767±150	<8	53±6	<4	<4	<5	22±5	11±6	<12	30±13	40±16	33±15
Q9335-3e	opx	25.8	27.5	11.3	<42	17±5	263±5	<6	25±3	7±3	31±3	37±4	26±6	19±8	81±11	92±13
Q9335-5e	ol	44.9	13.0	6.7	966±78	<8	24±9	7±4	10±4	7±6	11±6	14±7	121±18	<13	17±20	147±36
Q9335-8e	ol	40.2	22.8	1.6	<33	<11	110±4	8±3	<7	<7	<8	<8	<11	<13	31±10	<30
Q9338-1e	cpx	30.2	17.2	17.2	<43	128±10	117±4	10±2	—	—	20±4	<8	23±6	<13	31±14	<36
Q9342-1e	opx	20.5	37.1	7.0	<765	28±7	340±5	59±3	116±6	—	51±4	56±5	17±5	18±7	90±9	347±18
Q9345-2e	ol	44.5	19.6	0.5	35±28	<9	189±7	37±4	—	—	9±3	<7	27±7	<14	30±10	<24
Q9329-4e	ol	47.5	15.4	1.7	126±106	<7	68±9	<4	—	—	14±7	16±8	<11	20±19	<18	29±23
Q9304-1e	opx	37.9	21.7	5.0	<206	<8	49±5	62±5	—	—	7±5	<7	19±10	24±13	47±17	59±16

Table 4 continued

Sulphide	Host	Fe %	Ni %	Cu %	Zn	As	Se	Mo	Ru	Rh	Pd	Ag	Sn	Sb	Te	Pb
<i>Intergranular (24)</i>																
QL27-1i	39.8	23.3	1.5	<27	13±6	153±17	8±3	17±5	6±3	23±5	14±4	20±8	<13	29±11	<22	
QL27-2i	33.1	18.5	13.0	113±61	<9	124±14	<5	8±4	<6	10±5	15±7	38±9	<14	<18	57±14	
QL27-3i	33.0	28.6	3.0	35±22	<10	128±13	<6	18±5	<6	10±4	54±12	24±9	22±9	<16	26±14	
QL27-5i	35.7	20.4	8.6	133±62	<9	108±8	5±3	13±4	<5	17±5	23±7	40±14	<13	34±17	44±22	
QL27-7i	41.1	18.8	4.7	242±29	138	78±8	<5	<5	<5	<5	22±7	93±14	18±12	<19	43±19	
QL27-8i	38.5	21.4	4.7	44±58	<8	92±5	8±3	<5	<5	<6	19±6	20±10	15±11	<19	22±20	
QL27-9i	40.7	21.0	3.0	<33	<10	147±4	8±2	16±3	<6	15±3	9±4	35±7	15±7	27±8	29±11	
QL27-10i	37.6	16.3	10.7	661±71	<9	151±7	7±4	14±6	<6	11±5	28±7	24±13	24±14	39±17	<23	
QL27-11i	33.0	16.0	15.7	210±81	<8	140±7	<5	<5	<5	17±5	26±6	42±13	26±12	36±15	78±15	
Q9321-4i	38.6	21.8	4.1	113±60	<10	74±9	10±6	<5	9±10	9±8	19±13	34±18	69±23	69±29	46±25	
Q9321-7i	51.3	10.4	3.0	188±105	38±24	83±23	18±20	22±25	<5	7±25	<6	64±52	<12	226±77	71±57	
Q9321-8i	56.1	6.9	1.6	3948±118	51±28	50±21	14±16	—	—	38±26	<7	72±55	174±84	69±90	29±67	
Q9321-16i	39.2	17.3	8.2	<36	<10	82±4	10±2	<6	<7	<7	7±3	15±6	20±7	18±14	<27	
Q9321-17i	34.7	12.8	17.1	47±120	<8	81±6	<5	<5	<6	<7	<8	<13	<16	<20	35±24	
Q9335-2i	34.7	21.7	8.2	72±75	<8	64±9	<4	12±9	<6	11±9	<7	55±21	50±38	<21	163±28	
Q9335-4i	22.2	41.5	0.9	<35	<11	87±3	9±2	14±2	<7	9±2	8±3	18±5	19±5	30±7	<29	
Q9335-7i	27.9	33.0	3.7	<29	<9	87±5	6±3	10±3	<6	17±4	12±4	30±8	<12	40±12	74±13	
Q9345-1i	36.3	23.6	4.7	80±50	<9	111±5	36±3	—	—	21±4	11±4	15±7	16±8	30±9	41±10	
Q9345-3i	40.1	21.5	3.0	<30	18±6	105±7	22±5	—	—	86±8	13±5	15±9	<15	49±18	26±15	
Q9329-2i	19.6	43.7	1.4	—	<11	112±6	8±3	13±4	<7	16±4	—	—	—	<23	202±20	
Q9329-3i	37.7	25.8	1.1	—	<12	151±5	15±3	29±3	<7	15±4	—	—	—	33±10	52±17	
Q9329-5i	30.4	26.5	7.7	<219	<12	80±8	<6	—	—	<8	48±12	134±24	37±27	87±35	114±34	
Q9304-2i	30.9	29.2	4.5	—	<10	111±7	52±5	<6	6±3	<6	—	—	—	<19	31±17	

MDL: Zn 20–812, As 6–15, Se 4–10, Mo 3–7, Ru 4–8, Rh 4–8, Pd 4–9, Ag 5–10, Sn 10–16, Sb 12–18, Te 15–25, Pb 15–45. Errors for major elements: Fe <2%, Ni <1.5%, Cu <10%.

Table 5: Proton microprobe analyses of sulphide grains in pyroxenites

Sulphide	Host	Fe %	Ni %	Cu	Zn	As	Se	Mo	Ag	Sn	Sb	Te	Pb
<i>Enclosed (51)</i>													
QL2-5e	cpx	61.8	1.39	3561 ± 112		<11	35 ± 4	<6	<9		<16		<30
QL2-6e	cpx	62.8	0.62	755 ± 32		<10	37 ± 4	7 ± 3	<8	18 ± 5		33 ± 9	<28
QL2-7e	cpx	62.5	0.93	1136 ± 39		<10	39 ± 3	7 ± 2	<8				<28
QL2-9e	cpx	62.1	0.82	6172 ± 175		<10	36 ± 3	7 ± 2	16 ± 5	123 ± 9		<17	48 ± 13
QL2-14e	sp	61.0	1.33	1.24% ± 142	<28	<10	37 ± 3	7 ± 3	12 ± 4	<13	<15	<18	<27
QL2-15e	cpx	60.1	1.80	1.70% ± 359		<31	28 ± 10		<30	79 ± 23		<76	<86
QL2-16e	sp	61.3	1.11	1.21% ± 155	1660 ± 69	<16	17 ± 5	<8	<15	79 ± 14	41 ± 15	64 ± 19	<44
QL2-18e	cpx	62.5	0.96	747 ± 23	<22	<10	37 ± 3	<6	<8	63 ± 10	<13	<15	31 ± 13
QL2-21e	cpx	63.0	0.45	953 ± 56		12 ± 6	36 ± 4	8 ± 2	16 ± 4	81 ± 9	12 ± 6	<17	<27
QL2-22e	cpx	62.8	0.77	191 ± 27	<28	<10	36 ± 4	5 ± 2	15 ± 3	67 ± 8			<27
QL2-23e	sp	62.4	1.07	1331 ± 37		<10	35 ± 5	7 ± 2	<8	15 ± 5	<14	18 ± 8	<26
QL2-24e	cpx	62.9	0.63	171 ± 28		<10	39 ± 4	8 ± 2	9 ± 3	23 ± 6	<15	<18	<27
QL2-25e	cpx	62.4	0.90	2037 ± 32		<10	34 ± 4	6 ± 2	195 ± 3	35 ± 7	<15	<17	<27
QL3-1e	cpx	62.4	1.06	1261 ± 64		<13	35 ± 4	<7	<11	1134 ± 30		<24	42 ± 14
QL3-2e	cpx	62.7	0.85	<104		<10	38 ± 3	<5	<7			23 ± 7	32 ± 11
QL3-4e	cpx	62.9	0.65	<90		<9	35 ± 3	8 ± 2	9 ± 3	16 ± 5	18 ± 6		<25
QL7-1e	cpx	62.3	1.12	860 ± 87		<15	30 ± 5		<12	54 ± 12	<27		<42
QL7-2e	cpx	62.7	0.78	779 ± 63		<11	36 ± 5	6 ± 2	<8	24 ± 6	<16	<19	<31
QL7-3e	cpx	61.0	0.49	2.19% ± 414	<286		<38		<55	196 ± 48		<154	
QL7-4e	cpx	62.2	1.21	1837 ± 125	<93	<28	27 ± 8	13 ± 8		115 ± 23	<53	99 ± 35	<77
QL7-5e	cpx	61.3	1.38	9614 ± 132		<25	38 ± 8		<24	<44	61 ± 24		<67
QL7-6e	cpx	62.8	0.63	1275 ± 150	271 ± 54	<45	38 ± 16		<44	816 ± 58	131 ± 44		<125
QL7-7e	cpx	62.4	0.89	2405 ± 112		<32	42 ± 10	<20		<55	<70	<91	<87
QL7-8e	sp	62.5	0.68	3353 ± 108	2387 ± 94	<18	19 ± 5	<11	<277	<36	47 ± 19	77 ± 29	<51
QL7-9e	cpx	62.1	1.19	2814 ± 130	<147	<50	64 ± 15	<24	<37		<77	<103	<136
QL7-10e	sp	62.7	0.60	2211 ± 101	2757 ± 116			<11	<23		<50	80 ± 28	<53
QL15-4e	sp	63.2	0.36	<105	3805 ± 154	<20	<16	<15	<29	<62	<78		<56
QL15-7e	cpx	62.2	0.89	5079 ± 157	247 ± 52	<47	<36		109 ± 24	236 ± 66	<125		<131
QL15-10e	cpx	61.8	1.08	7117 ± 135	<100	<35	<27			<74	<94		<98
QL15-14e	sp	63.0	0.45	1217 ± 57	3220 ± 127	<19	<14		<24	53 ± 21	73 ± 37	<75	<52
QL15-15e	cpx	61.7	1.40	4727 ± 201	206 ± 55	<46	40 ± 14	<32	<58	177 ± 56	<152	<194	<130
QL15-16e	cpx	61.0	1.93	6333 ± 149	<93	<32	<24	<23	<34	134 ± 56	195 ± 56		<88
QL17-1e	sp	62.2	1.05	2713 ± 60	457 ± 26	<12	28 ± 4	8 ± 3	<11	30 ± 165	<28	<36	
QL17-2e	sp	61.0	1.52	1.07% ± 226	1116 ± 56	<13	33 ± 5	<8		36 ± 13		<48	<37

Table 5 continued

Sulphide	Host	Fe %	Ni %	Cu	Zn	As	Se	Mo	Ag	Sn	Sb	Te	Pb
OL17-3e	sp	61.6	1.06	9295±244	3616±140	<18	15±8			52±21	<60	152±35	<50
OL18-1e	sp	62.6	0.72	1864±88	3279±133	<23	<17	<14	<31	<60			<59
OL18-2e	cpx	59.2	1.72	2.75%±440		45±15	32±5	11±4	<16	163±17		77±20	<45
OL18-3e	sp	62.0	1.00	5254±117	114±20	<11	27±4	8±2	<9	85±8	18±8	<23	<30
OL18-4e	cpx	62.1	1.30	1226±52		<11	36±5	8±3	<10	<17	<21	<28	<30
OL18-5e	sp	62.2	1.07	3227±76	2057±83	<18	17±5	<11	<20	41±17	<46	<61	<48
OL18-6e	sp	61.6	1.27	7237±131	392±33	<12	29±4	11±3		23±8	<23	<29	<32
OL18-7e	cpx	62.3	0.84	4031±187	<30	<11	36±4	<6	15±4	50±10	<19		<31
OL18-8e	cpx	58.0	1.65	4.13%±587		<13	34±4	<7	<11	<19	<24		<35
OL18-9e	cpx	58.6	4.23	7837±155		<17	29±8	10	<16	39±17	45±20		<46
OL21-1e	cpx	61.2	1.55	7948±161	<105	<29	34±5	<132	158±12	422±23	<29	71±35	72±17
OL21-2e	cpx	61.0	1.24	1.39%±243		<22	<23	<18	75±13	120±26			<81
OL21-3e	cpx	61.4	1.56	5825±189		<22	37±7		<20		<48		<61
OL21-4e	cpx	57.2	4.44	2.03%±467		<25	69±11	<13	<18	<37			336±34
OL21-5e	cpx	61.3	1.09	1.23%±289	<226	<48	40±16	<27	45	333±48	<111		<132
OL21-6e	cpx	61.2	1.83	5627±178		<27	42±9	<17	26±11	191±34	<52	<69	<74
O9355-1e	cpx	60.6	2.49	5269±189		<12	64±5	9±3	9±4	224±12	<16		<32
<i>Intergranular (13)</i>													
OL2-8i		57.7	4.12	1.88%±220	200±25	<14	38±4	29±4	14±5	95±11	<22		<38
OL2-13i		56.8	4.59	2.35%±243	382±36	<17	35±5	37±5	19±7	<27		<41	<48
OL2-17i		62.8	0.45	3366±68			42±4	7±4	<8	23±6	15±7	17±8	
OL2-20i		61.8	1.03	7256±116			37±4	9±3	17±4	20±6	<15		36±10
OL3-3i		63.4	0.12	<63	<31	2396±50	27±4	498±10	<10	<16	32±10	<24	<210
OL7-11i		63.4	0.14	<205	294±43	<469	37±12	<24	<43	215±39	<41	<119	<114
OL15-1i		61.1	1.74	7526±234	79±32	<16	37±5	<10	29±8	59±15	<40	91±27	<46
OL15-5i		60.4	2.58	6081±123	164±20	<12	41±4	<12	42±6	126±12	38±12	53±15	101±17
OL15-6i		59.8	2.70	1.10%±156	484±41	<19	26±6	<12	88±11	973±39	<53		95±19
OL15-8i		61.7	1.38	5426±166	1643±90	<24	33±7	<17	49±15	119±30	126±35	94±43	<69
OL15-11i		60.9	1.68	1.06%±218	351±39	17±6	35±4	8±3	63±7	1725±43	<33		142±15
OL15-12i		59.3	3.07	1.25%±203	343±27	16±8	34±5	15±5	24±8	52±16	<45		<45
OL15-13i		60.9	1.96	7495±157	1469±65	<15	27±6	<10	21±8				<42

All concentrations expressed in parts per million except where noted otherwise. Errors for major elements (Fe, Ni) are <2% of the measured values. MDL (lowest, ppm): Fe 220, Cu 42, Ni 96, Zn 21, As 9, Se 7, Mo 5, Ru 6, Pd 6, Ag 7, Sn 9, Sb 12, Te 15, Pb 25. MDL (highest, ppm): Fe 2557, Cu 471, Ni 602, Zn 286, As 470, Se 39, Mo 132, Ru 32, Pd 38, Ag 277, Sn 124, Sb 152, Te 194, Pb 210.

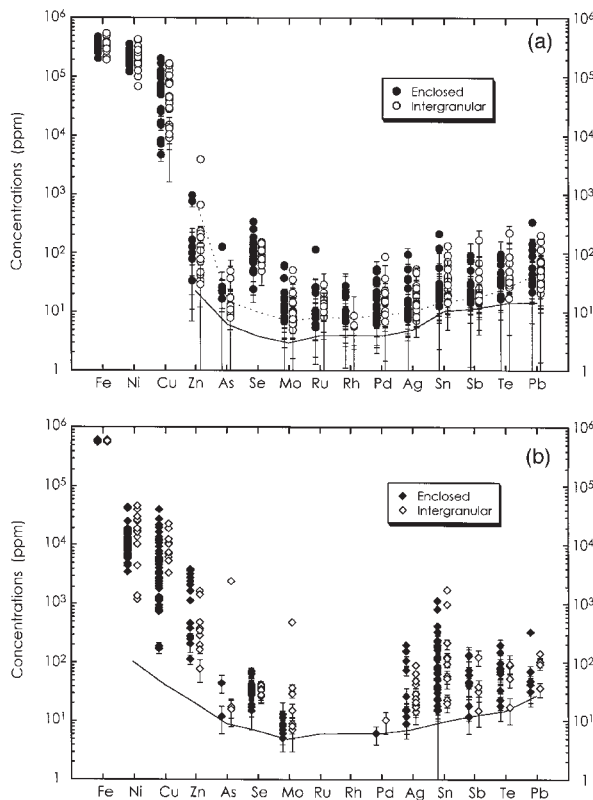


Fig. 8. Major and trace element concentrations determined using proton microprobe. (a) Lherzolite-hosted sulphides; (b) pyroxenite-hosted sulphides. The minimum detection limit is shown in continuous line for each trace element. The broken line indicates the raised detection limit when the best counting statistics is not achieved. The elements are arranged in the order of atomic number (see Table 4 for detection limits).

(1987) and Szabó & Bodnar (1995). Sulphide grains from pyroxenite samples contain much less Ni than those from lherzolites (Fig. 9). The Cu contents of sulphide grains in lherzolite samples vary from 0.5 to 20.5 wt %, but most display <9 wt % Cu. This range of Cu values reflects the highly variable presence of chalcopyrite in the assemblage (Fig. 10). In contrast, all sulphide minerals from pyroxenite samples contain <4 wt % Cu. In these samples Cu contents appear to be coupled with As, Mo and Pb. Co abundance is not obtained from the routine proton microprobe data reduction procedure because of peak overlaps. The Co contents of individual sulphide grains range from 0.2 to 0.7 wt % in lherzolite samples, but are <0.4 wt % in pyroxenite samples. If Zn is detected (Fig. 8), there is a marked difference between the compositions of sulphide grains in lherzolite versus pyroxenite samples. The former is <1000 ppm (except for one grain), whereas the latter ranges to 4000 ppm (Fig. 9). The Zn-rich sulphide grains from pyroxenite samples contain less Ni, Cu and Se, but more Fe than

those that are Zn poor. This may be a fractionation trend inherited during sulphide precipitation.

The sulphide grains from lherzolite samples range between 24 and 340 ppm of Se, but most grains contain 40–160 ppm. Sulphide grains from pyroxenite samples contain between 25 and 45 ppm of Se (Fig. 9). Bulanova *et al.* (1996) found that sulphide inclusions in peridotitic diamonds show a bimodal Se distribution with one peak near 50 ppm and the other between 110 and 160 ppm. Those workers reported that sulphide inclusions in eclogitic diamonds contain about 50 ppm Se. The Se contents of our sulphide grains resemble those of sulphide inclusions in diamond. Arsenic is either below our detection limit of 6–15 ppm, or ranges from 10 to 30 ppm. A single matrix grain in a pyroxenite sample (QL3-3i, Table 5) that contains 2396 ppm As is probably not a mantle feature.

Although PGE were found in some lherzolite-hosted sulphide mineral grains, PGE were not detected in the pyroxenite-hosted sulphide mineral grains (Fig. 9). The PGE contents of sulphide mineral grains in lherzolite samples vary from below detection limits (6–8 ppm) to several tens of ppm; the highest values found are ~110 ppm Ru and ~90 ppm Pd in analyses Q9342-1e and Q9345-3i, respectively. However, most sulphide mineral grains contain <30 ppm of any single PGE. The positive correlations among the PGE, especially between Ru and Pd, suggest that the sulphide grains have suffered little from re-equilibration. Bulanova *et al.* (1996) reported PGE-free sulphide inclusions in eclogitic diamonds and PGE-bearing sulphide inclusions in peridotitic diamonds; the latter contain ~40–300 ppm Ru, ~20–170 ppm Rh and ~20–50 ppm Pd along with ~50–110 ppm Os and ~90–170 ppm Ir. The PGE values obtained by Bulanova *et al.* (1996) are generally higher than those we determined. A recent ICP-MS analysis of handpicked sulphide grains from orogenic spinel lherzolite samples yielded PGE contents of <4 ppm for each element (Pattou *et al.*, 1996).

The heavy elements (Mo, Ag, Sn, Sb, Te and Pb) are present in various quantities in the sulphide mineral grains (Fig. 9). Except for Ag, the contents of these elements are similar in the lherzolite- and pyroxenite-hosted sulphide mineral grains. There are weak positive correlations among Ag, Sb, Te and Pb. Mo ranges from 5 to 62 ppm, with most values between 5 and 20 ppm (Fig. 9). One pyroxenite sulphide grain shows exceptionally high Mo content of ~500 ppm. In one sulphide mineral grain (Q9342-1e) a high Mo content (59 ppm) is coupled with the highest Ru (116 ppm) measured as well as a high Pd content (51 ppm). However, another high-Mo sulphide (Q9304-1e) has low PGE contents. The Mo contents of sulphide mineral grains we measured are significantly lower than the 50–100 ppm of sulphide inclusions found in diamonds (Bulanova *et al.*, 1996).

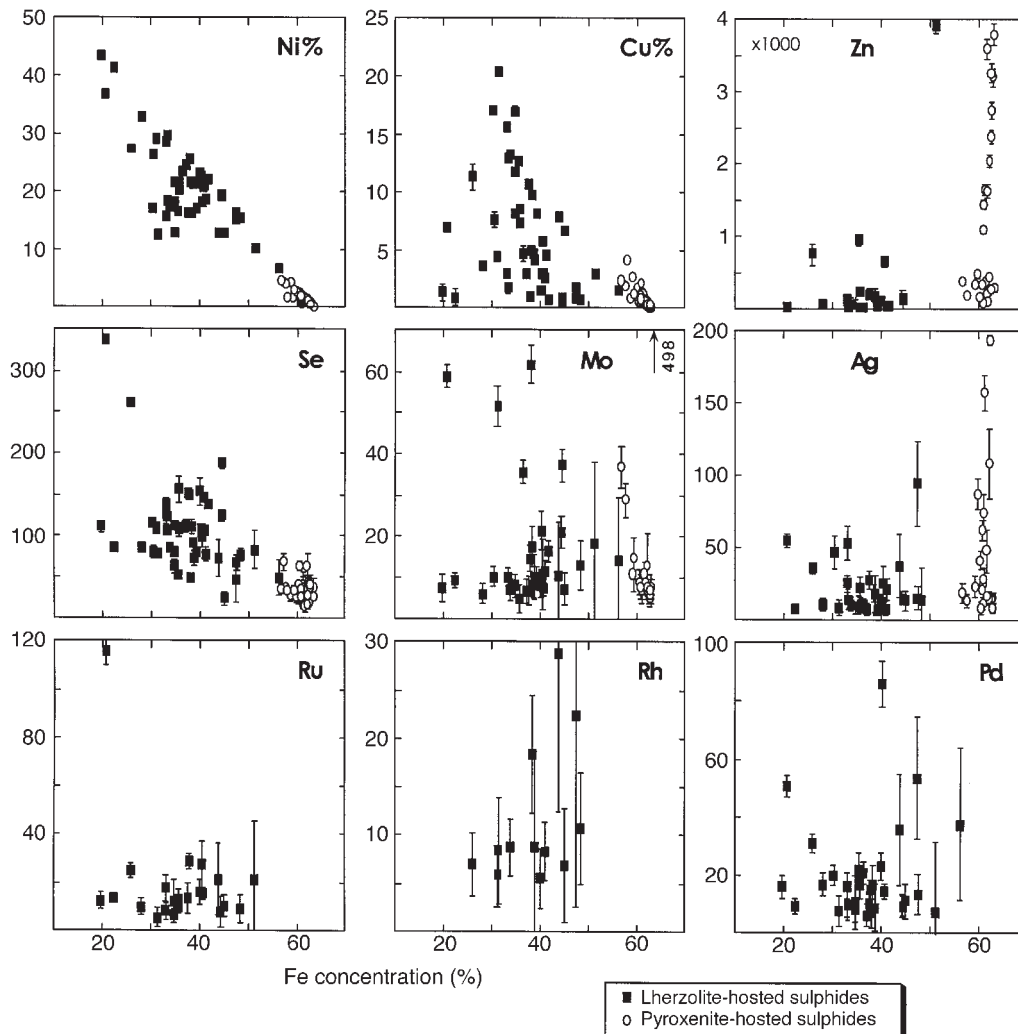


Fig. 9. Element plots against Fe for bulk sulphide compositions. Concentrations in ppm except where noted otherwise. Errors of measurements are displayed when the uncertainties are larger than the size of the plot symbols.

Most sulphide mineral grains from lherzolite samples contain Ag but two-thirds of sulphide mineral grains from pyroxenite samples lack Ag. In contrast, pyroxenite-hosted sulphide minerals display higher maximum Ag contents (Fig. 9). However, most sulphides, regardless of host rock type, contain <100 ppm Ag, clustering around 8–40 ppm. Both the lherzolite- and pyroxenite-hosted sulphide minerals contain significant amounts of Sn. Most lherzolite-hosted sulphide mineral grains contain <60 ppm of Sn, whereas the pyroxenite-hosted ones range from 20 to 240 ppm. Sn of several hundred to thousand ppm may reflect contamination from a tin lap wheel used for polishing. Sb, Te and Pb occur at similar levels regardless of the host rock type. Sb ranges up to 80 ppm, with most samples <40 ppm. Te contents of the sulphide mineral grains are in general <100 ppm, and most grains display <80 ppm of Pb.

DISCUSSION

The Cu–Fe–Ni–S system at various temperatures

In the Cu–Fe–Ni–S system, the monosulphide phase FeS crystallizes on the Fe–S join at 1192°C (Fig. 10). Upon cooling, Ni and Cu increase in the FeS phase to form the monosulphide solid solution (MSS) $(\text{Fe},\text{Ni})_{1-x}\text{S}$, which contains <5 wt % Cu and up to 14 wt % Ni at 1100°C (see Table 6). With further cooling, the MSS field expands as more Cu dissolves in it, and the sulphide liquid becomes rich in Ni. At 1000°C, a maximum Ni/Fe ratio of ~3.3 is reached by the MSS. This corresponds to a non-metal deficient monosulphide containing 14 wt %

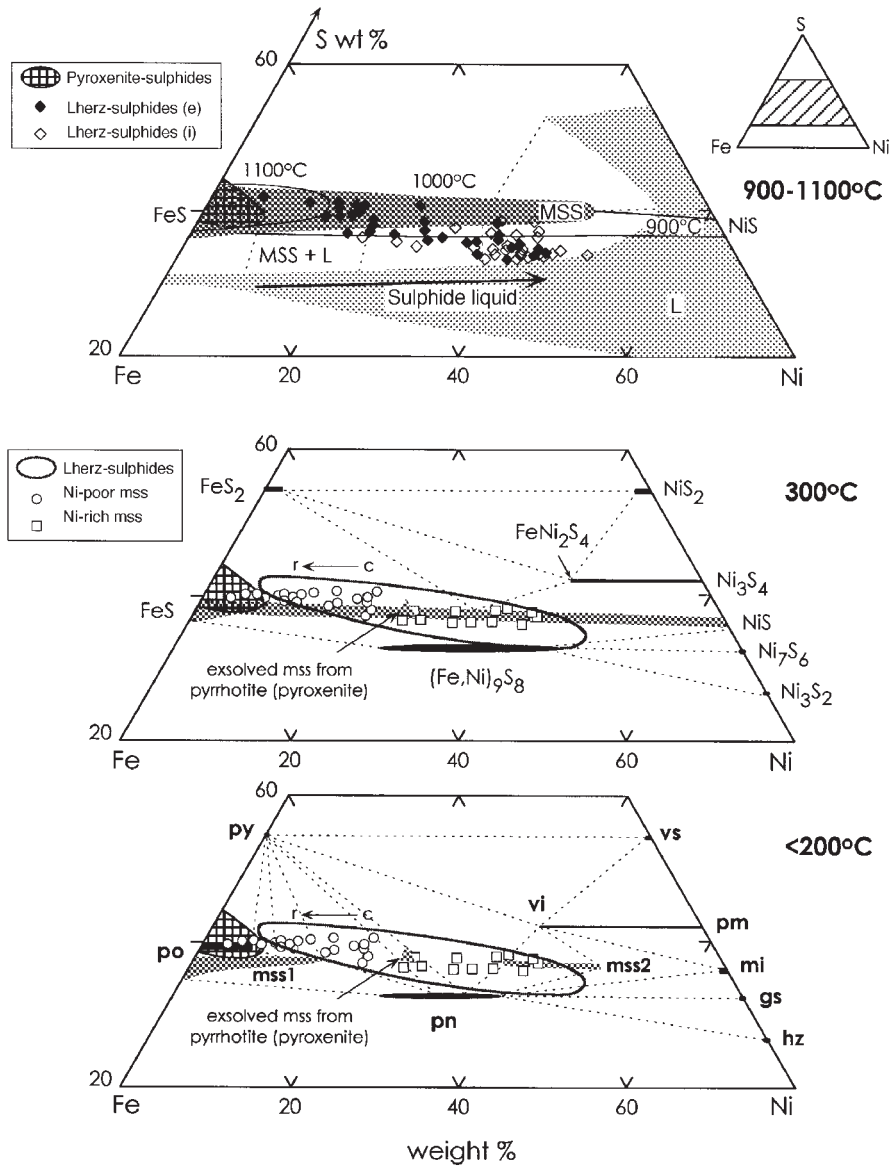


Fig. 10. The bulk sulphide compositions plotted on the Fe–Ni–S ternary system. Plotted data are reconstituted bulk compositions based on EMP analyses of individual phases. The bulk compositions of lherzolite-hosted sulphides (enclosed and intergranular) are shown by diamond symbols in the 900–1100°C phase diagram. The EMP-identified Ni-poor and Ni-rich monosulphides in the polyphase sulphide grains in lherzolites are plotted in the 300°C phase diagram for comparison. The high-temperature (1100–900°C) phase relations are taken from Kullerud *et al.* (1969), with the 1000°C fields highlighted by shade. The phase diagrams at 300°C and <200°C are taken from Craig (1973). In the <200°C phase diagram, mss1 and mss2 are the experimentally established fields for Ni-poor and Ni-rich monosulphide solid solutions. Compositions illustrated are: pentlandite (pn), (Fe,Ni)₉S₈; violarite (vi), FeNi₂S₄; vaesite (vs), NiS₂; polydymite (pm), Ni₃S₄; millerite (mi), NiS; godlevskite (gs), Ni₇S₆; heazlewoodite (hz), Ni₃S₂; pyrite (py), FeS₂; pyrrhotite (po), FeS; Ni-poor monosulphide (mss1), (Fe,Ni)S; Ni-rich monosulphide (mss2), (Ni,Fe)S. MSS is the first phase to crystallize in the system and its field expands across the entire Fe–Ni–S system from 1100 to 900°C. At the ambient temperature of the mantle xenoliths (<1015°C), the Qilin lherzolite sulphides encompass both MSS and MSS + L fields, indicating partial crystallization of the immiscible sulphide melt with the residue liquid enriched in Ni. Rayleigh fractionation calculation suggests an MSS/liquid ratio of 90:10 for the Qilin mantle sulphides. The polyphase sulphide assemblages in Qilin lherzolite sulphides comprise phases such as pn, mi, hz, mss1, mss2 and py, suggesting subsolidus re-equilibration of the high-*T* MSS at temperatures not more than 300°C. It is likely that the assemblages have not reached final equilibrium.

Fe, 46 wt % Ni, 7 wt % Cu and 33 wt % S in equilibrium with a sulphide liquid containing 44 wt % Ni, 15 wt % Cu, 7 wt % Fe and 34 wt % S. Chalcopyrite begins to

crystallize from the liquid at 960°C. The MSS–bornite and MSS–chalcopyrite tie lines are established at about 930–940°C. At 900°C, the MSS stability field spans the

Table 6: Extracted sulphide chemistry information based on the experimentally determined phase relations in the Fe–Ni–Cu–S system (Kullerud et al., 1969)

T (°C)	MSS		Bo	Chp	Sulphide liquid composition			
	Ni max. (%)	Cu max. (%)	Fe max. (%)	M/S ratio	Fe (%)	Ni (%)	Cu (%)	S (%)
1100	14	5	11		43	17	6	34
1000	46	7	22		6	54	20	20
940	—	7.5	32	>1	—	—	—	—
900	60	6	26	>1				
700	60	3	17	>1				
650	11*	3	17	>1				
635	—			<i>solidus</i>	—			
550	7*	<3	—	>1				
200	<15, Ni-poor mss,† >30, Ni-rich mss			~1‡				
<200				<1				

MSS, monosulphide solid solution; Bo, bornite; Chp, chalcopyrite; M/S, metal/sulphur; —, no information can be extracted.
 *MSS coexisting with pyrite (\pm chalcopyrite).
 †Craig (1973).
 ‡Yund & Kullerud (1966).

entire system. About 6 wt % Cu can be dissolved in the MSS at this temperature. At $\sim 860^\circ\text{C}$, $(\text{Ni,Fe})_3\text{S}_2$ crystallizes from the sulphide liquid, which saturates the system in sulphur. The MSS at this temperature has more restricted metal/sulphur ratios than higher-temperature MSS (Karup-Møller & Makovicky, 1995). With further cooling, the solubility of Fe in the $(\text{Ni,Fe})_3\text{S}_2$ solid solution decreases. This solid solution phase remains on the liquidus until all sulphide liquid is consumed (at $\sim 635^\circ\text{C}$). At $\sim 740^\circ\text{C}$, pyrite becomes stable together with MSS and chalcopyrite. At 610°C , the MSS and the $(\text{Ni,Fe})_3\text{S}_2$ phase react to form pentlandite, which remains stable at lower temperatures. This pentlandite varies widely in composition (Graterol & Naldrett, 1971; Misra & Fleet, 1973). The high-temperature $(\text{Ni,Fe})_3\text{S}_2$ phase converts to heazlewoodite at 556°C . The MSS field spans the system at temperature $>380^\circ\text{C}$ (Craig, 1973). Below 380°C , Ni-rich MSS decomposes to form stoichiometric NiS, which ultimately converts to millerite and/or polydymite (Ni_3S_4) at lower temperature. Below 300°C , MSS exsolves into Ni-poor (mss1) and Ni-rich (mss2) monosulphide solid solutions and pentlandite; the solvus between mss1 and mss2 low- T phases centres around 33–35 wt % Fe (Craig, 1973; Misra & Fleet, 1973). At 200°C , the Ni content of re-equilibrated mss1 is <15 wt %, whereas mss2 contains >30 wt % Ni (Craig, 1973).

The nature of sulphide mineral grains in the mantle and their re-equilibration

In the ternary Fe–Ni–S system the reconstructed compositions of lherzolite-hosted sulphide mineral grains show Ni/Fe ratios from 0.1 to 2.8, whereas compositions of pyroxenite-hosted sulphide mineral grains lie near the FeS end of the MSS (Fig. 10). Xu *et al.* (1996) reported that the ambient temperatures of Qilin xenoliths range from 900 to 1015°C for lherzolite samples and from 1090 to 1150°C for pyroxenite xenoliths. At such temperatures, MSS is the only possible solid phase in the Cu–Fe–Ni–S system. Compositions of pyroxenite sulphide minerals lie within the MSS field only, but the lherzolite sulphide minerals are in both the MSS and MSS + L fields (Fig. 10).

Compositions of lherzolite-hosted matrix sulphide minerals lie only within the MSS + L field. In contrast, compositions of sulphide mineral inclusions from lherzolite samples span the MSS and MSS + L fields. This suggests that the early crystallized MSS was incorporated into surrounding silicates as solid inclusions and the residual sulphide liquid was trapped between the larger silicate mineral grains that make up these rocks. The initial and final compositions of the fractionating sulphide liquid were approximately $\text{Fe}_{66}\text{Ni}_8\text{S}_{26}$ (wt %) and $\text{Fe}_{29}\text{Ni}_{44}\text{S}_{27}$ (wt %), respectively. This represents a Ni enrichment of ~ 12 times relative to Fe with virtually un-

changed S (Fig. 10). Li *et al.* (1996) showed that both Ni and Cu behave incompatibly in the MSS–sulphide liquid system under S-undersaturated conditions. At 1000–1100°C, Ni partitioning between MSS and sulphide liquid approaches 0.28 (average of four measurements). By solving the Rayleigh fractionation equation, $f^{D-1} = C_1/C_0$ (where f is the residue mass fraction of liquid, D is the crystal–liquid partition coefficient, C_1 is the concentration of element in the fractionated liquid and C_0 is the concentration of element in the original liquid), we obtain $f = 0.09$. Thus, about up to 90% of the sulphide melt crystallized into the MSS that occurs as inclusions in other lherzolite minerals.

The pyroxenite samples show evidence that sulphide liquid was entirely, completely crystallized and that all sulphide grains reflect the ambient temperature (~1100°C) of the xenolith population. Because the initial crystallization temperature of the Ni-free MSS (pyrrhotite, FeS) is 1192°C, the mafic magmas that became pyroxenite xenoliths must have been at temperatures $\geq 1200^\circ\text{C}$ in the upper mantle, because sulphide liquids evidently were segregated from the silicate magmas, crystallized and trapped in the silicate mineral grains.

Pentlandite is a major constituent of lherzolite-hosted sulphide mineral grains. Because pentlandite is stable in the Fe–Ni–S system only at temperatures below 610°C, the multiphase assemblages are not of primary mantle origin. Chalcopyrite also is a common phase in the lherzolite-hosted sulphide mineral grains. MSS and chalcopyrite (chp) can coexist only at temperatures below ~340°C because the MSS–chp tie-line is established in the Cu–Fe–S system at these conditions (Kullerud *et al.*, 1969). Thus the equilibration temperature of the sulphide assemblage is limited to $\leq 340^\circ\text{C}$. Pentlandite is not associated with pyrite in the sulphide grains we studied (except in one matrix grain in sample Q9321, Table 1), which suggests equilibration above the MSS unmixing temperature of 300°C (Fig. 10).

The two monosulphide mineral solid solutions recognized in the polyphase assemblages appear to form a continuous series (Fig. 10). The higher M/S ratios of the Ni-rich MSS [which resemble those of the mss2 of Craig (1973)], probably indicate a structural deviation from the Ni-poor MSS [mss1 of Craig (1973)] before the onset of complete unmixing. Because the data for the MSS encompass the entire immiscibility region expected at temperatures $< 300^\circ\text{C}$ (Craig, 1973), these phases are best explained as metastable products formed at a temperature of ~300°C. Heazlewoodite from lherzolite-hosted sulphide mineral grains contains 1.2–3.1 wt % Fe, more similar to the high-temperature (Ni,Fe)₃S₂ solid solution (maximum Fe soluble ~3.5 wt % at 650°C; Kullerud *et al.*, 1969) than to the re-equilibrated low- T equivalent that is virtually Fe free. Millerite is stable only below 250°C (Craig, 1973). In summary, the sulphide

mineral assemblages in lherzolite xenoliths are products of subsolidus re-equilibration of high-temperature MSS. Most of the sulphide mineral phases we studied suggest re-equilibration temperatures of ~300°C following (post-eruption) cooling of the xenoliths in the volcanic host rocks. It is likely that these assemblages have not reached equilibrium.

Mantle sulphide minerals in peridotite vs pyroxenite samples

Sulphide minerals in peridotitic rocks are thought to originate from immiscible sulphide melts trapped during partial melting events in the mantle residues (e.g. Frick, 1973; Dromgoole & Pasteris, 1987; Szabó & Bodnar, 1995; and references therein), whereas pyroxenite-hosted sulphide minerals (as well as sulphide inclusions within clinopyroxene megacrysts) are attributed to sulphur saturation during the crystallization of mafic magmas in the mantle (e.g. Andersen *et al.*, 1987; Dromgoole & Pasteris, 1987). Sulphide mineral inclusions in diamond are interpreted as primordial mantle sulphides (Bulanova *et al.*, 1996) or as precipitates from an S,C-rich fluid associated with early igneous events in the mantle (Bulanova, 1995; Deines & Harris, 1995).

The experimentally determined liquidus phase relationships in the system FeS–FeO–Fe₃O₄–SiO₂ show that sulphide and silicate liquids are immiscible near 1100°C (MacLean, 1969). The coexisting silicate and sulphide liquids at such a temperature can dissolve substantial amounts of FeS (16 wt %) and oxides (e.g. FeO 15 wt %, SiO₂ 1.5 wt %, Fe₃O₄ 0.5 wt %), respectively, according to MacLean (1969). Partial melting of mantle materials that contain ~200–300 ppm sulphur (a commonly accepted value for the subcontinental mantle, e.g. O'Neill, 1991; Keays, 1995) would yield a primary silicate melt and an immiscible sulphide melt if the degree of melting (mass fraction) is less than ~25% (Keays, 1995). Modelling of trace element patterns of clinopyroxene from Qilin lherzolite samples suggests that <10% of melting occurred in the upper mantle of the Qilin region (Xu *et al.*, 1999). An 'immiscible sulphide melt' may segregate and settle to the bottom of the melting zone as a result of its higher density and subsequently be incorporated into residual mantle rocks. Documentation of a carbonatite–sulphide–silicate melt assemblage in depleted peridotites from the Canary Islands supports the 'immiscible sulphide melt' hypothesis, although that triple-melt assemblage may be related to metasomatic activity, rather than to partial melting in the upper mantle (Kogarko *et al.*, 1995).

The 'immiscible sulphide melt' hypothesis was partly based on the rounded appearance of most sulphide mineral inclusions in the silicate minerals of peridotites.

Dromgoole & Pasteris (1987) summarized the argument about the possible genesis of lherzolite-hosted sulphide minerals in a study of xenoliths from Kilbourne Hole, New Mexico (USA). They concluded that no contamination mechanism can explain the occurrence and chemistry of all lherzolite-hosted sulphide minerals at Kilbourne Hole. Szabó & Bodnar (1995) also concluded that sulphide minerals in unmetasomatized peridotite xenoliths from eastern Europe represent immiscible melts trapped during partial melting. They considered that the immiscible Cu–Ni-bearing sulphide melt was in equilibrium with MSS at high temperatures.

Our data on the Qilin xenoliths indicate that both inclusions and matrix grains of sulphide minerals in lherzolite samples have broadly similar bulk compositions, with the latter being rich in Ni. The difference between the two textural and compositional types can be modelled by a fractionation process, in which early MSS crystals are trapped in silicates, and Cu, Ni-rich sulphide melt is subsequently trapped between silicate and oxide mineral grains. The origin of the pyroxenite-hosted sulphide mineral grains appears more clear-cut than that of the peridotite-hosted ones. Because the melting of sulphide minerals occurs at lower temperatures than the melting of silicate minerals, the sulphides are the first mineral phases to melt in the mantle. Keays (1995) demonstrated that all partial melts of silicate minerals are saturated with sulphur if the degree of melting (mass fraction) is <25%, which is the case for most mafic magmas. The change of physical conditions or fractional crystallization of silicate and oxide phases of a rising mantle melt could form a second generation of sulphide minerals in a closed mafic system.

In the Qilin pyroxenite xenoliths, sulphide minerals occur only as inclusions in clinopyroxene and spinel grains. Both clinopyroxene and spinel exhibit a bimodal distribution of *mg*-number, and the sulphide minerals are found in host grains with lower *mg*-number (Fig. 2). Low *mg*-number, sulphide-bearing spinel grains are poorer in Cr than high *mg*-number, sulphide-barren spinels, which typically contain >1 wt % of Cr₂O₃. These observations indicate that such sulphide mineral grains crystallized at a late stage of magmatic evolution. The lack of sulphide mineral inclusions in orthopyroxene and garnet grains reflects the origin of the latter two phases via exsolution from primary, high-temperature clinopyroxene during post-emplacement cooling of the pyroxenites to the ambient mantle geotherm (Griffin *et al.*, 1984; Xu *et al.*, 1996).

Effects of mantle metasomatism upon sulphide mineral grains

The Qilin xenolith suite has undergone some mantle metasomatism, as shown by the presence of primary

amphibole and carbonate in some lherzolite samples. Some K–Fe–Ni sulphide minerals in kimberlite-hosted mantle xenoliths are derived from metasomatic fluids or melts (e.g. Clarke *et al.*, 1977). Such sulphide minerals were not detected in our study of 40 thin sections of spinel lherzolite xenoliths from Qilin. Nevertheless, it is possible that some sulphide mineral droplets that are associated with fluid inclusions and fracture planes may have formed by remobilization of primary sulphide minerals during mantle metasomatism. These small (<10 µm) blebs are rich in Cu but poor in Ni compared with the larger sulphide grains that we think represent primary mantle sulphide minerals.

Szabó & Bodnar (1995) described sulphide mineral inclusions in metasomatically derived amphibole grains in an equigranular, metasomatized peridotite. Those workers interpreted the sulphide grains to reflect sulphur saturation of a mantle-derived andesitic melt that served as the metasomatic agent. However, the bulk composition of the 'metasomatic sulphide' of Szabó & Bodnar (1995) resembles that of sulphide mineral inclusions in the same xenolith suite that are interpreted to be primary mantle sulphide minerals. Furthermore, phase equilibrium considerations require that if the amphibole-hosted sulphide mineral inclusions were derived from an andesite-like mantle melt, their composition should be similar to those of the pyroxenite-hosted sulphide minerals we studied. The metasomatic sulphide of Szabó & Bodnar (1995) contains up to 12.3 wt % of Ni; the pyroxenite sulphide grains (>50) in the Qilin xenolith suite we analysed contain <4 wt % Ni (Table 5). Thus, the reported chemistry of the metasomatic sulphide of Szabó & Bodnar (1995) is inconsistent with an origin from a mafic to intermediate silicate melt.

The solubility of oxygen in sulphide minerals

Oxygen is ubiquitous in the Qilin sulphide minerals. Ninety-five percent of the lherzolite-hosted sulphide minerals we analysed contain up to 1.6 wt % oxygen. Sulphide minerals from pyroxenite xenoliths contain up to 1.1 wt % oxygen (Table 2). Both lherzolite- and pyroxenite-hosted sulphides contain an average amount of 0.6 wt % oxygen, which corresponds to 0.5–3 formula percent of oxygen in the sulphide minerals. Experimental studies have found soluble oxygen in sulphide melt at various pressures. There are generally about 1–3 formula percent of oxygen in high-pressure (3–15 GPa) sulphide liquids of eutectic composition in the Fe–FeO–FeS system (e.g. Wendlandt & Huebner, 1979; Urakawa *et al.*, 1987). The amount of dissolved oxygen in sulphide liquid increases to around 19 formula percent at 1 atm pressure (Naldrett, 1969). However, the relationship between pressure and oxygen solubility in sulphide liquid is complex.

Doyle & Naldrett (1987) argued that natural Fe–S–O liquids that form sulphide–magnetite ores must have maintained an O/S ratio near 1:1 based on calibrated oxygen and sulphur fugacity data. They further argued that the discrepancy between this theoretical analysis and the fact that most magmatic ores contain <10% magnetite further suggests the loss of oxygen to early crystallizing olivine in a mafic or ultramafic magma.

If the analysis by Doyle & Naldrett (1987) is correct, the mantle sulphide minerals we studied should have lost almost all the oxygen they contained to silicate minerals after equilibration in either the melting or the emplacement region. The unmixing of oxide and sulphide in single discrete inclusions in pyroxenite would further suggest inhomogeneous oxygen–sulphide separation in the mantle (Fig. 4f).

Implications for the origin of diamond

Diamonds contain two suites of genetically related inclusions, which are termed peridotitic and eclogitic suites. Knowledge of the chemistry of these inclusions allows reconstruction of the environment and conditions of diamond growth in the mantle (e.g. Gurney *et al.*, 1984; Boyd *et al.*, 1985; Meyer, 1987; Griffin *et al.*, 1992).

Sulphide inclusions in diamond are assigned to either the peridotitic or eclogitic suites based on the presence and absence of specific silicate and/or oxide mineral inclusions in the same diamond (e.g. Bulanova, 1995). However, problems arise if only sulphide inclusions are found, which is the most common situation. Peridotitic diamonds were thought to contain sulphide minerals with Ni contents of 16.5–29.8 wt %, whereas the sulphide minerals in eclogitic diamonds yielded Ni values of 0.5–8.2 wt % (Yefimova *et al.*, 1983). Recent trace element analyses of sulphide mineral inclusions in Yakutian diamonds refined this proposal (Bulanova *et al.*, 1996), but left the provenance of Siberian sulphide mineral inclusions, containing 11–18 wt % of Ni, in doubt. Furthermore, the Ni contents of sulphide inclusions in South African diamonds vary almost continuously from ~1 to ~35 wt % with no clear break (Deines & Harris, 1995). Without a clear distinction between peridotitic and eclogitic sulphide minerals based on chemical composition, one has to rely on the rare occurrence of other mineral inclusions.

Our compositional data for sulphide minerals from lherzolite and pyroxenite xenoliths may provide a petrological basis for the interpretation of sulphide minerals that occur as inclusions in diamond. The lherzolite sulphide minerals contain 10–44 wt % Ni with most between 12 and 30 wt % (Fig. 11). The pyroxenite sulphide minerals contain <4.5 wt % of Ni, and average 1.4 wt %. It is apparent that if the lherzolite and pyroxenite sulphide minerals we studied are analogous to peridotitic

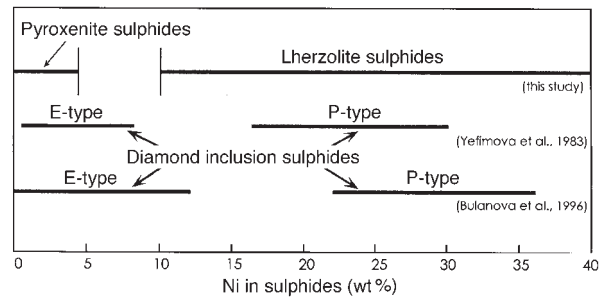


Fig. 11. The Ni concentration ranges of the xenolith sulphides and diamond inclusion sulphides. E-type, eclogitic diamond inclusion suite; P-type, peridotitic diamond inclusion suites.

and eclogitic suite sulphide inclusions in diamonds, sulphide minerals that contain >10 wt % of Ni are of peridotitic origin, whereas those with <4.5 wt % Ni are of mafic–eclogitic origin.

CONCLUSIONS

Detailed petrographic observations and microprobe analyses have shown that sulphide minerals are common minor phases of the upper mantle, but that their origin is complex. Sulphide minerals in lherzolitic xenoliths are rich in Ni and Cu, and some contain some PGE, whereas those in pyroxenitic xenoliths are poor in Ni and Cu and contain no PGE. The origin of mantle sulphide minerals is closely related to the petrogenesis of their respective host rocks. The lherzolite-hosted sulphide minerals probably represent immiscible sulphide melts trapped during partial melting of the mantle. The pyroxenite-hosted sulphide minerals probably reflect sulphur saturation during the crystallization of a mafic magmas. The structural state and composition of mantle sulphide minerals depend on the ambient temperature conditions. Partially crystallized sulphide melt may be present in much of the upper mantle.

ACKNOWLEDGEMENTS

This paper was completed while the first author was the recipient of the Australian Post-Doctoral Research Fellowship (Australian Research Council). The mineral analyses were carried out with the assistance of Norm Pearson (electron microprobe), Chris Ryan and Tin Tin Win (proton microprobe). The study was also supported by a Research Grant to J.G. and S.Y.O'R. under the ARC Small Grants Scheme. Other financial support included Macquarie University internal and DEET-TIL grants. We thank Tom Andersen, Jill Pasteris and Steven Shirey for thorough and constructive reviews of the

manuscript, and are especially grateful for Sorena Sorensen's careful attention in editing, all of which has contributed greatly to the quality improvement of the paper. This is Publication 145 from the Key Centre for Geochemical Evolution and Metallogeny of Continents (GEMOC).

REFERENCES

- Andersen, T., Griffin, W. L. & O'Reilly, S. Y. (1987). Primary sulfide melt inclusions in mantle-derived megacrysts and pyroxenites. *Lithos* **20**, 279–294.
- Bell, P. M., England, J. L. & Kullerud, G. (1964). Pentlandite: pressure effect on breakdown. *Carnegie Institution of Washington Yearbook* **63**, 206–207.
- Bishop, F. C., Smith, J. V. & Dawson, J. B. (1975). Pentlandite–magnetite intergrowth in De Beers spinel lherzolite: review of sulfide in nodules. *Physics and Chemistry of the Earth* **9**, 323–337.
- Boyd, F. R., Gurney, J. J. & Richardson, A. (1985). Evidence for a 150–200 km thick Archean lithosphere from diamond inclusion thermobarometry. *Nature* **315**, 387–389.
- Bulanova, G. P. (1995). The formation of diamond. *Journal of Geochemical Exploration* **53**, 1–23.
- Bulanova, G. P., Griffin, W. L., Ryan, C. G., Shestakova, O. Ye. & Barnes, S.-J. (1996). Trace elements in sulfide inclusions from Yakutian diamonds. *Contributions to Mineralogy and Petrology* **124**, 111–125.
- Cabri, L. J. (1973). New data on phase relations in the Cu–Fe–S system. *Economic Geology* **68**, 443–454.
- Clarke, D. B., Pe, G. G., MacKay, R. M., Gill, K. R., O'Hara, M. J. & Gard, J. A. (1977). A new potassium–nickel sulfide from a nodule in kimberlite. *Earth and Planetary Science Letters* **35**, 421–428.
- Craig, J. R. (1973). Pyrite–pentlandite assemblages and other low temperature relations in the Fe–Ni–S system. *American Journal of Science* **273A**, 496–510.
- Deines, P. & Harris, J. W. (1995). Sulfide inclusion chemistry and carbon isotopes of African diamonds. *Geochimica et Cosmochimica Acta* **59**, 3173–3188.
- De Waal, S. A. & Calk, L. C. (1975). The sulfides in the garnet pyroxenite xenoliths from Salt Lake Crater, Oahu. *Journal of Petrology* **16**, 134–153.
- Desborough, G. A. & Czamanske, G. K. (1973). Sulfides in eclogite nodules from a kimberlite pipe, South Africa, with comments on violarite stoichiometry. *American Mineralogist* **58**, 195–202.
- Distler, V. V., Ilupin, I. P. & Laputina, I. P. (1987). Sulfides of deep-seated origin in kimberlites and some aspects of copper–nickel mineralization. *International Geological Review* **29**, 456–464.
- Doyle, C. D. & Naldrett, A. J. (1987). The oxygen content of 'sulfide' magma and its effect on the partitioning of nickel between coexisting olivine and molten ores. *Economic Geology* **82**, 208–211.
- Dromgoole, E. L. & Pasteris, J. D. (1987). Interpretation of the sulfide assemblages in a suite of xenoliths from Kilbourne Hole and Potrillo Maar, New Mexico. In: Morros, E. & Pasteris, J. D. (eds) *Mantle Metasomatism and Alkaline Magmatism. Geological Society of America, Special Paper* **215**, 25–46.
- Fleet, M. E. & Pan, Y. (1994). Fractional crystallization of anhydrous sulfide liquid in the system Fe–Ni–Cu–S, with application to magmatic sulfide deposits. *Geochimica et Cosmochimica Acta* **58**, 3369–3377.
- Fleet, M. E. & Stone, W. E. (1990). Nickeliferous sulfides in xenoliths, olivine megacrysts and basaltic glass. *Contributions to Mineralogy and Petrology* **105**, 629–636.
- Frey, F. A. & Prinz, M. (1978). Ultramafic inclusions from San Carlos, Arizona: petrological and geochemical data bearing on their genesis. *Earth and Planetary Science Letters* **38**, 129–176.
- Frick, C. (1973). The sulphides in griquaitite and garnet–peridotite xenoliths in kimberlite. *Contributions to Mineralogy and Petrology* **39**, 1–16.
- Graterol, M. & Naldrett, A. J. (1971). Mineralogy of the Marbridge No. 3 and No. 4 nickel–iron sulfide deposits, with some comments on low temperature equilibration in the Fe–Ni–S system. *Economic Geology* **66**, 886–900.
- Griffin, W. L., Wass, S. Y. & Hollis, J. D. (1984). Ultramafic xenoliths from Bullenmerri and Gnotuk maars, Victoria, Australia: petrology of a subcontinental crust–mantle transition. *Journal of Petrology* **25**, 53–87.
- Griffin, W. L., O'Reilly, S. Y. & Stabel, A. (1988). Mantle metasomatism beneath western Victoria, Australia, II: Isotopic geochemistry of Cr-diopside lherzolites and Al-augite pyroxenites. *Geochimica et Cosmochimica Acta* **52**, 449–459.
- Griffin, W. L., Gurney, J. J. & Ryan, C. G. (1992). Variations in trapping temperatures and trace elements in peridotite–suite inclusions from African diamonds: evidence for two inclusion suites and implications for lithosphere stratigraphy. *Contributions to Mineralogy and Petrology* **110**, 1–15.
- Gurney, J. J., Harris, J. W. & Rickard, R. S. (1984). Minerals associated with diamonds from the Roberts Victor Mine. In: Kornprobst, J. (ed.) *Kimberlites II: The Mantle and Crust–Mantle Relationships*. Amsterdam: Elsevier, pp. 25–32.
- Karup-Møller, S. & Makovicky, E. (1995). The phase system Fe–Ni–S at 725°C. *Neues Jahrbuch für Mineralogie, Monatshefte* 1–10.
- Keays, R. R. (1995). The role of komatiitic and picritic magmatism and S-saturation in the formation of ore deposits. *Lithos* **34**, 1–18.
- Kogarko, L. N., Henderson, C. M. B. & Pacheco, H. (1995). Primary Ca-rich carbonatite magma and carbonate–silicate–sulfide liquid immiscibility in the upper mantle. *Contributions to Mineralogy and Petrology* **121**, 267–274.
- Kullerud, G., Yund, R. A. & Moh, G. H. (1969). Phase relations in the Cu–Fe–S, Cu–Ni–S, and Fe–Ni–S systems. *Economic Geology, Monograph* **4**, 323–343.
- Li, C., Barnes, S.-J., Makovicky, E., Rose-Hansen, J. & Makovicky, M. (1996). Partitioning of nickel, copper, iridium, rhenium, platinum, and palladium between monosulfide solid solution and sulfide liquid: effects of composition and temperature. *Geochimica et Cosmochimica Acta* **60**, 1231–1238.
- Lorand, J. P. (1989). Abundance and distribution of Cu–Fe–Ni sulfides, sulfur, copper and platinum-group elements in orogenic-type spinel peridotites of Ariège (Northeastern Pyrenees, France). *Earth and Planetary Science Letters* **93**, 50–64.
- Lorand, J. P. (1991). Sulphide petrology and sulphur geochemistry of orogenic lherzolites: a comparative study of the Pyrenean bodies (France) and the Lanzo Massif (Italy). *Journal of Petrology* (Special Lherzolites Issue) 77–95.
- Lorand, J. P. & Conquéré, F. (1983). Contribution à l'étude des sulfures dans les enclaves de lherzolite à spinelle des basaltes alcalins (Massif Central, et Languedoc, France). *Bulletin de Minéralogie* **106**, 585–605.
- MacLean, W. H. (1969). Liquidus phase relations in the FeS–FeO–Fe₃O₄–SiO₂ systems and their application in geology. *Economic Geology* **64**, 865–884.
- Meyer, H. O. A. (1987). Inclusions in diamonds. In: Nixon, P. H. (ed.) *Mantle Xenoliths*. Chichester, UK: John Wiley, pp. 501–522.
- Meyer, H. O. A. & Boctor, N. Z. (1975). Sulfide–oxide minerals in eclogite from Stockdale kimberlite, Kansas. *Contributions to Mineralogy and Petrology* **52**, 57–68.

- Meyer, H. O. A. & Brookins, D. G. (1971). Eclogite xenoliths from Stockdale Kimberlite, Kansas. *Contributions to Mineralogy and Petrology* **34**, 60–72.
- Misra, K. C. & Fleet, M. E. (1973). The chemical compositions of synthetic and natural pentlandites. *Economic Geology* **68**, 518–539.
- Mitchell, R. H. & Keays, R. R. (1981). Abundance and distribution of gold, palladium and iridium in some spinel and garnet lherzolites: implications for the nature and origin of precious metal-rich intergranular components in the upper mantle. *Geochimica et Cosmochimica Acta* **45**, 2425–2442.
- Naldrett, A. J. (1969). A portion of the system Fe–S–O between 900 and 1080°C and its application to sulfide ore magmas. *Journal of Petrology* **10**, 171–201.
- O'Neill, H. St C. (1991). The origin and the early history of the Earth—a chemical model. Part 2: the Earth. *Geochimica et Cosmochimica Acta* **55**, 1159–1172.
- O'Reilly, S. Y. & Griffin, W. L. (1987). Eastern Australia—4000 kilometres of mantle samples. In: Nixon, P. H. (ed.) *Mantle Xenoliths*. Chichester, UK: John Wiley, pp. 267–280.
- Pattou, L., Lorand, J. P. & Gros, M. (1996). Non-chondritic platinum-group element ratios in the Earth's mantle. *Nature* **379**, 712–715.
- Peterson, R. & Francis, D. (1977). The origin of sulfide inclusions in pyroxene megacrysts. *American Mineralogist* **62**, 1049–1051.
- Rudnick, R. L., Eldridge, C. S. & Bulanova, G. P. (1993). Diamond growth history from *in situ* measurement of Pb and S isotopic compositions of sulfide inclusions. *Geology* **21**, 13–16.
- Ryan, C. G., Cousens, D. R., Sie, S. H., Griffin, W. L. & Suter, G. F. (1990). Quantitative PIXE microanalysis of geological material using the CSIRO proton microprobe. *Nuclear Instruments and Methods* **B47**, 55–71.
- Szabó, C. S. & Bodnar, R. J. (1995). Chemistry and origin of mantle sulfides in spinel peridotite xenoliths from alkaline basaltic lavas, Nógrád–Gömör Volcanic Field, northern Hungary and southern Slovakia. *Geochimica et Cosmochimica Acta* **59**, 3917–3927.
- Urakawa, S., Kato, M. & Kumazawa, M. (1987). Experimental study of the phase relations in the system Fe–Ni–O–S up to 15 GPa. In: Manghnani, M. H. & Syono, Y. (eds) *High-Pressure Research in Mineral Physics*. Tokyo: Terra; Washington, DC: American Geophysical Union, pp. 95–111.
- Usselman, T. M. (1975). Experimental approach to the state of the core: Part I. The liquidus relations of the Fe-rich portion of the Fe–Ni–S system from 30 to 100 kb. *American Journal of Science* **275**, 278–290.
- Vakhrushev, V. A. & Sobolev, N. V. (1973). Sulfidic formations in deep xenoliths from kimberlite pipes in Yakutia. *International Geological Review* **15**, 103–110.
- Wendlandt, R. F. & Huebner, J. S. (1979). Melting relations of portion of the system Fe–S–O at high pressure and applications to composition of the Earth's core. *Lunar and Planetary Science* **X**, 1329–1331.
- Xu, X., O'Reilly, S. Y., Zhou, X. & Griffin, W. L. (1996). A xenolith-derived geotherm and the crustal/mantle boundary at Qilin, southeastern China. *Lithos* **38**, 41–62.
- Xu, X., O'Reilly, S. Y., Griffin, W. L. & Zhou, X. M. (1999). Genesis of young lithospheric mantle in southeastern China: a LAM-ICPMS trace element study. *Journal of Petrology* (submitted).
- Yefimova, E. S., Sobolev, N. V. & Pospelova, L. N. (1983). Inclusions of sulfides in diamonds and their paragenesis. *Zapiski Vsesoyuznogo Mineralogicheskogo Obshchestva* **112**, 300–310.
- Yund, R. A. & Kullerud, G. (1966). Thermal stability of assemblages in the Cu–Fe–S system. *Journal of Petrology* **7**, 454–488.
- Zhao, H. (1985). Petrological characteristics of the mantle-derived pyroxenite xenoliths from Qilin, Puning County, Guangdong Province (in Chinese with English abstract). *Acta Petrologica Sinica* **1**, 23–33.